

Age and deposition of the Fort Crittenden Formation: A window into Late Cretaceous Laramide and Cenozoic tectonics in southeastern Arizona

Emilia A. Caylor^{1,†}, Barbara Carrapa¹, Kurt Sundell¹, Peter G. DeCelles¹, and Joshua M. Smith²

¹University of Arizona, 1040 East 4th Street, Tucson, Arizona 85719, USA

²Northern Arizona University, 624 South Knoles Drive, Flagstaff, Arizona 86011, USA

ABSTRACT

The Upper Cretaceous Fort Crittenden Formation exposed in the Santa Rita and Huachuca Mountains of southeastern Arizona is a syntectonic deposit that has been associated with Laramide tectonic activity. However, the spatio-temporal relationships among Cretaceous sedimentation, magmatism, basement exhumation, and possible flat slab-related processes in the southern Laramide region remain poorly understood. Age controls for uplift and erosion of local topography and syntectonic deposition in response to deformation remain particularly poor. The Fort Crittenden Formation comprises 800–2500 m of locally derived fluvial to alluvial fan sedimentary rocks and records paleodrainage reorganization in response to active tectonics. Changes in sedimentary facies, provenance, and paleoflow suggest deposition in a tectonically partitioned intraforeland basin. New detrital zircon data constrain the timing of deposition of the Fort Crittenden Formation between ca. 86 Ma and ca. 76 Ma. The lack of depositional age zircons throughout the majority of the Fort Crittenden Formation is consistent with a magmatic lull in the Cordilleran arc between ca. 90 Ma and ca. 76 Ma. The overlying Salero Formation and Late Cretaceous intrusions are expressions of renewed magmatism in southeastern Arizona at ca. 75 Ma. New Lu-Hf data indicate that magmas evolved from contamination of old juvenile crust. When interpreted in conjunction with other regional data sets, our study indicates that the Laramide deformation front migrated eastward into southwestern New Mexico by 75 Ma. Thermal modeling of apatite fission track and (U-Th)/He data from granitic

clasts are consistent with Late Cretaceous–Paleocene (ca. 76–55 Ma) heating related to magmatism and cooling and exhumation during the Eocene and Oligocene.

INTRODUCTION


The Laramide tectonic event took place during Late Cretaceous–Eocene time and encompasses the region from Montana through northern Sonora, Mexico. Signature features of the Laramide event include basement-involved uplifts that disrupted the regional Cordilleran foreland basin up to ~1000 km inboard of the plate margin and eastward migration of arc magmatism, which have been explained by flat slab subduction (Fig. 1; Coney, 1972; Coney and Reynolds, 1977; Cross and Pilger, 1978; Dickinson, 1989; Saleeby, 2003). Mechanisms of slab flattening responsible for the Laramide event are a subject of much debate, with two hypotheses receiving the most attention. One attributes the flat slab to subduction of a buoyant ridge (Cross and Pilger, 1978; Henderson et al., 1984; Saleeby, 2003; Liu et al., 2008, 2010), and the other attributes the flat slab to increased rates of plate convergence and enhanced intraplate shear stresses (Coney, 1972; Snyder et al., 1976; Coney and Reynolds, 1977; Dickinson and Snyder, 1978; Jordan, 1981; Livaccari et al., 1981; Chapin and Cather, 1983; Bird, 1984, 1998; Engebretson et al., 1984; Tarduno et al., 1985; Jordan and Allmendinger, 1986; Erslev, 1993; Constenius, 1996; DeCelles, 2004; Humphreys, 2009; Jones et al., 2011; Humphreys et al., 2015). These mechanisms are not mutually exclusive (e.g., Cross and Pilger, 1978; Liu et al., 2010).

The southern extent of the Laramide province encompasses the region south of the Colorado Plateau in southern California, Arizona, New Mexico, and northern Sonora, Mexico, and deformed as early as the Late Cretaceous (Dickinson, 1989; Dickinson et al., 1989; Lawton, 2008; Clinkscales and Lawton, 2015, 2018).

The relationships between Laramide tectonics, basin development, and magmatism in the southern Laramide province remain problematic due to poor age constraints, poorly understood deformation styles, and the paucity of data on regional basin development (Titley, 1976; Davis, 1979; Reynolds, 1980; Krantz, 1989). Although basement-involved structures and isolated clastic deposits have been associated with Laramide tectonics in southern Arizona, the relationships between basement exhumation and basin evolution remain largely unconstrained (Fig. 1; Drewes, 1972b; Titley, 1976; Davis, 1979; Reynolds, 1980; Krantz, 1989; Dickinson, 1989; Dickinson et al., 1989; Saleeby, 2003; Grove et al., 2003; Jacobson et al., 2007; Barth et al., 2008; Lawton, 2008; Chapman, 2017; Favorito and Sedorff, 2017; Holk et al., 2017). Furthermore, the potential connections between the Late Cretaceous (ca. 77–68 Ma) Pelona-Orocopia-Rand schist subduction complex associated with flat slab subduction and Laramide deposition in southeastern Arizona remain unexplored (Seymour et al., 2018; Chapman et al., 2018). Evidence of Laramide deformation throughout the southern Laramide province has been influenced and obscured by Cenozoic extensional tectonics, which has made understanding the tectonic evolution of the southern Laramide region and its relationship to the tectonic evolution of the North American Cordillera as a whole difficult.

Synorogenic sedimentary rocks and overlying volcanic units are scattered across southern Arizona, southwestern New Mexico, and Sonora, Mexico, and provide a unique opportunity for tracking early Laramide deformation, synorogenic deposition, and its relation to magmatism. These strata were deposited in local basins in response to Laramide tectonics and are referred to as the Fort Crittenden Formation and its equivalents in southeastern Arizona (Figs. 2 and 3; Hayes and Drewes, 1978; Hayes, 1986; Keith and Wilt, 1986; Inman, 1987; Dickinson, 1989; Dickinson et al., 1989). Mesozoic and Cenozoic paleogeography and stratigraphy in southeastern

[†]caylor.emilia@gmail.com.

Emilia Caylor  <http://orcid.org/0000-0001-8235-7190>

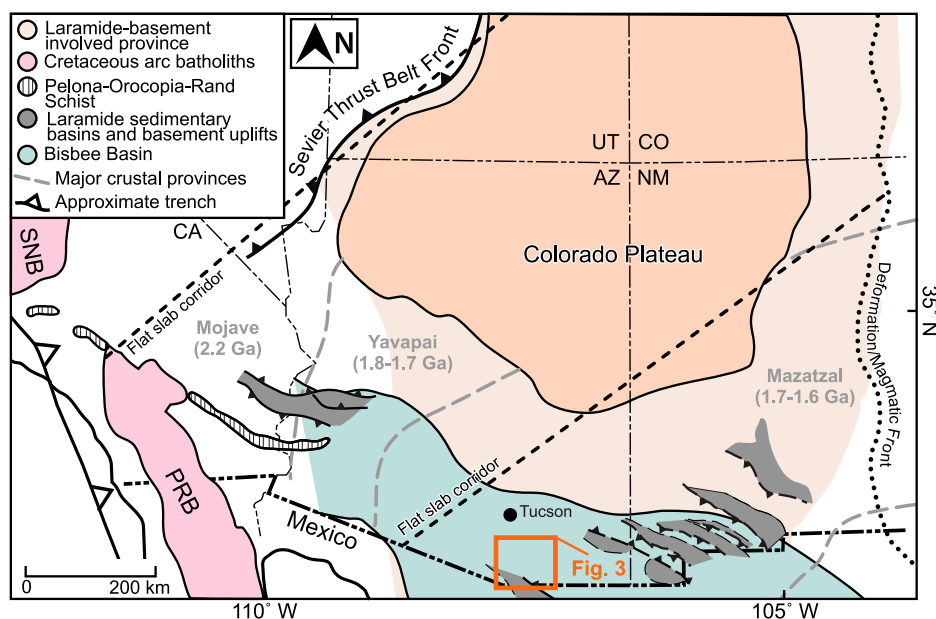


Figure 1. Map of southwest U.S. shows major crustal provinces (gray dashed lines), distribution of major Cretaceous arc batholiths (SNB—Sierra Nevada; PRB—Peninsular Range batholiths), Laramide magmatic/deformation front (black dotted line), the front of the Sevier fold and thrust belt, extent of the Colorado Plateau, Laramide basement-involved province, the Bisbee Basin, extent of the the Pelona-Orocopia-Rand schist, and Laramide sedimentary basins and basement uplifts (Dickinson et al., 1988; Dickinson and Lawton, 2001; Saleeby, 2003; DeCelles, 2004; Whitmeyer and Karlstrom, 2007; Jacobson et al., 2007; Lawton, 2008; Liu et al., 2010; Weil and Yonkee, 2012; Axen et al., 2018; Lawton et al., 2020). Dashed black lines indicate locations of the flat slab corridor according to Weil and Yonkee (2012). Study site location is marked by the orange rectangle (Fig. 3).

Arizona, the age of uplift and erosion of local topography, and deposition of Laramide syntectonic deposits such as the Fort Crittenden Formation remain sparsely documented. This study presents new sedimentological, provenance, geo-thermochronological (U-Pb and low-T thermochronology), and geochemical data (Lu-Hf isotopic analyses) that are able to constrain the timing, basin evolution, and tectonic setting of the Cretaceous Fort Crittenden Formation in the Santa Rita Mountains and Huachuca Mountains of southeastern Arizona, thus helping to understand the connections between Laramide tectonics and flat slab subduction processes in the southern Laramide region.

GEOLOGIC SETTING OF SOUTHEASTERN ARIZONA

The southwestern U.S. Cordillera is a classic example of a Cordilleran-type orogenic system that formed as a result of Mesozoic and Cenozoic tectonics associated with the subduction of the Farallon oceanic plate under continental North America (Krebs and Ruiz, 1987; Dickinson, 2004; Dickinson and Gehrels, 2008; DeCelles,

2004). This resulted in emplacement of intrusive igneous rocks and deposition of volcanic rocks related to Cordilleran arc magmatism in California, southern Arizona, and Sonora as early as the Late Triassic (Dickinson, 1989, 2004; Dickinson and Lawton, 2001; Cecil et al., 2011; Riggs et al., 2020). In the Santa Rita Mountains, Late Triassic–Jurassic volcanic rocks include the Mount Wrightson Formation (ca. 220–180 Ma) and the Gardner Canyon Formation (ca. 210 Ma; Fig. 3; Drewes, 1971b, 1976; Marvin et al., 1973; Riggs and Busby-Spera, 1990; Asmerom et al., 1990; Dickinson, 2003). Associated plutonic rocks include the Piper Gulch Monzonite (ca. 188 Ma) and the Squaw Gulch Granite (ca. 184 Ma and 170 Ma) (Drewes, 1976; Asmerom et al., 1990; Mizer, 2018). Early to mid-Jurassic (ca. 180–160 Ma) volcanic rocks in the Canelo Hills and Huachuca Mountains include the Canelo Hills volcanic rocks and unnamed siliceous volcanic sequences (Fig. 3; Hayes, 1970b; Krebs and Ruiz, 1987).

The Late Jurassic southwestern U.S. Cordillera is characterized by waning phases of arc magmatism and continental rifting associated with the opening of the Gulf of Mexico. Initia-

tion of rifting along the Sabinas-Chihuahua-Bisbee rift belt resulted in short-lived rift magmatism and widespread syntectonic sedimentation, e.g., the Bisbee Group (Figs. 1 and 2; Krebs and Ruiz, 1987; Dickinson et al., 1989; Busby-Spera et al., 1990; Dickinson and Lawton, 2001; Spencer et al., 2011). The Bisbee Group comprises ~3–4 km of marine and nonmarine syntectonic sedimentary rocks deposited during Late Jurassic rifting and Early Cretaceous post-extension thermal subsidence (Figs. 2 and 3; Dickinson, 1989). Deposition of the upper Bisbee Group continued until the mid-Cretaceous, when the southwestern U.S. Cordillera transitioned into a contractional tectonic setting (Dickinson and Lawton, 2001; Spencer et al., 2011; Martini et al., 2014; Lawton et al., 2020).

Starting with the Upper Jurassic Morrison Formation, the southwestern U.S. Cordillera developed a retroarc foreland basin system adjacent to the southern extension of the Cordilleran fold-and-thrust belt and the Sabinas-Chihuahua-Bisbee rift belt (Dickinson et al., 1989; Drewes, 1991; Tosdal and Stone, 1994; Barth et al., 2004; Spencer et al., 2011). Farther to the south in New Mexico and Arizona, a foreland basin started no later than ca. 110 Ma (Lawton et al., 2020). Upper Cretaceous locally derived, synorogenic sedimentary rocks in southeastern Arizona unconformably overlie the Bisbee Group and are suggested to record sedimentation in intermontane basins as a result of contractional deformation during early phases of Laramide tectonics (Fig. 2; Drewes, 1978; Davis, 1979; Dickinson, 1989). These deposits are referred to as the Fort Crittenden Formation and are exposed in the Santa Rita and Huachuca Mountains and its equivalents in other ranges including the Silver Bell, Tucson, Santa Catalina, Winchester, Pedregosa, and Chiricahua Mountains in southeastern Arizona (Fig. 3; Hayes, 1970a; Hayes, 1986; Hayes and Drewes, 1978; Lindberg, 1987).

In the Santa Rita Mountains, the Fort Crittenden Formation is divided into four members from bottom to top: the basal shale, lower red conglomerate, brown conglomerate, and upper red conglomerate members (Figs. 2C and 3B; Drewes, 1971b; Hayes, 1986; Dickinson et al., 1989). In the Huachuca Mountains, the Fort Crittenden Formation is divided into two members from bottom to top: the conglomerate member and the upper shale member (Figs. 2C and 3C; Hayes, 1970b). Previous estimates for the timing of deposition of the Fort Crittenden Formation are limited and are based on Santonian–Maastriichtian paleontological content within the basal shale member and Campanian (72.5 ± 2.2 Ma) K–Ar isotopic dating of biotite in the conformably overlying Salero Formation volcanic rocks

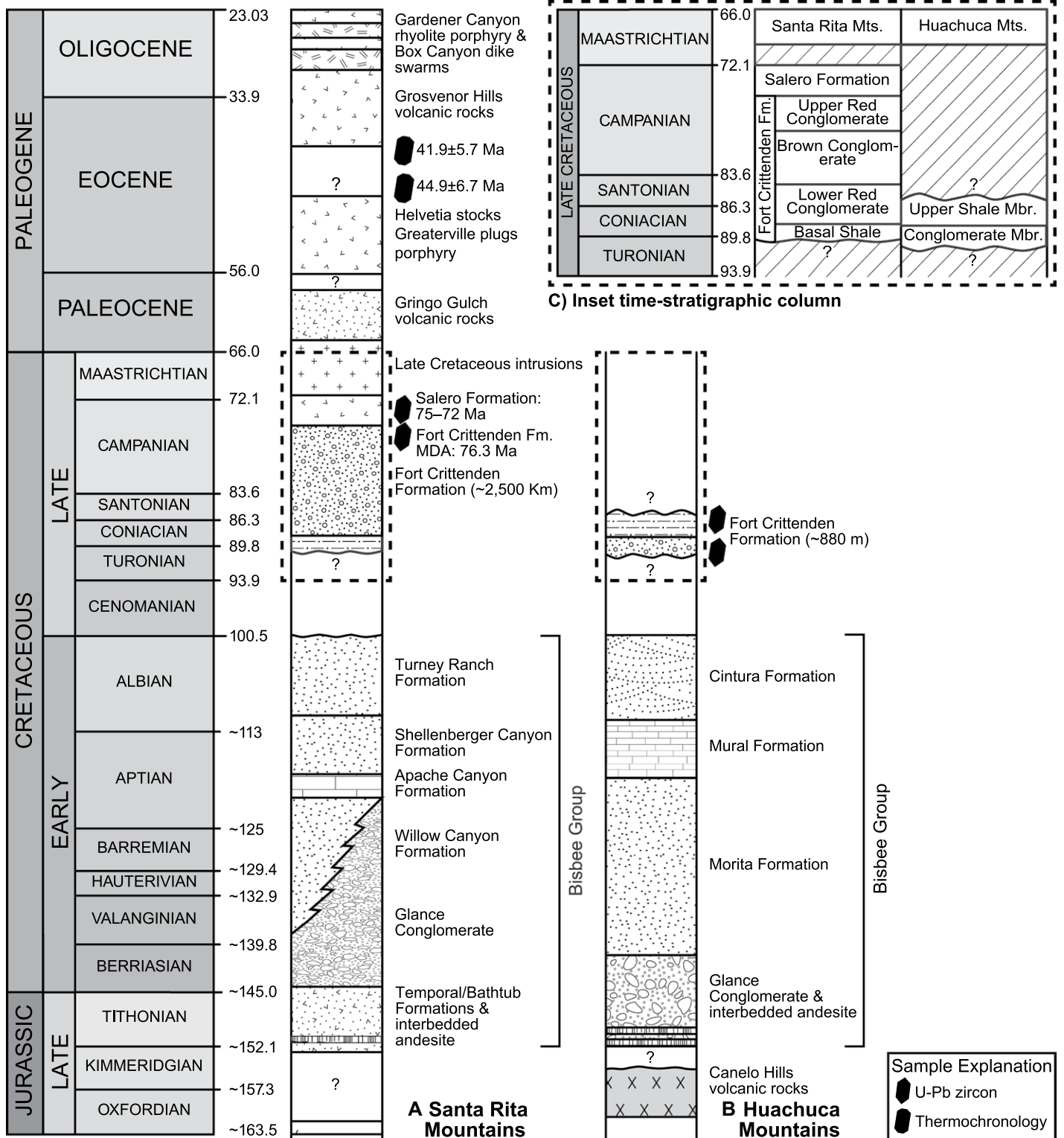


Figure 2. Time-stratigraphic columns are shown for Late Jurassic–Miocene section in the (A) Santa Rita Mountains and the (B) Huachuca Mountains. Modified after Hayes (1970b, 1970a, 1986); Drewes (1971a, 1976); Hayes and Drewes (1978); Krebs and Ruiz (1987); Inman (1987); Dickinson et al. (1989); Asmerom et al. (1990); Bassett and Busby (2005). The Geologic Timescale is after Walker et al. (2018). U-Pb zircon and thermochronologic samples are marked on stratigraphic columns (A and B).

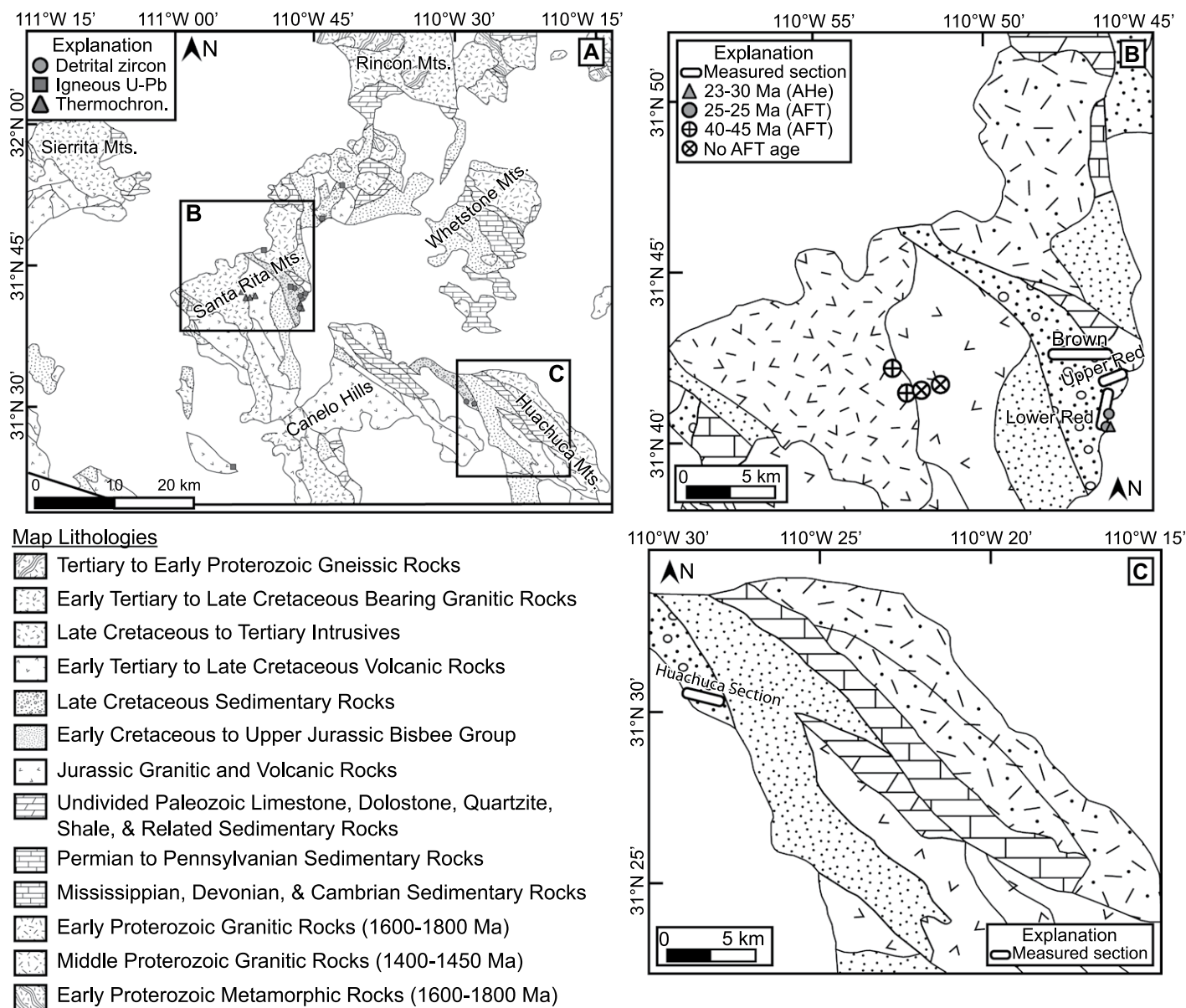


Figure 3. (A) Outset geologic map of southeastern Arizona shows boxes around inset geologic maps, detrital zircon, igneous U-Pb, and thermochronologic sample locations. Inset geologic maps of the study areas with locations of measured sections of the Fort Crittenden Formation and samples in the (B) Santa Rita Mountains (modified from Drewes, 1971a) and (C) Huachuca Mountains (modified from Hayes and Raup, 1968).

in the Santa Rita Mountains (Drewes, 1971b; Hayes, 1986; Inman, 1987).

The basal shale member is poorly exposed along the eastern flank of the Santa Rita Mountains and comprises five subunits that have been interpreted as lake margin and open lacustrine deposits (Drewes, 1971b; Hayes, 1986; Inman, 1987). Fossils in the basal shale member include freshwater gastropods, bivalves, turtles, freshwater fish, iguanodontid, and dinosaur fossils (Stoyanow, 1949; Miller, 1964; McCord, 1997; Dalman et al., 2018). Dinosaur fossils include Hadrosaurs, Theropods, and the most recently discovered

Crittendenceratops (Stoyanow, 1949; Miller, 1964; McCord, 1997; Heckert et al., 2003; Lucas and Heckert, 2005; Dalman et al., 2018). Fossil content within the basal shale member estimates a Santonian (ca. 86 Ma) maximum depositional age for the base of the Fort Crittenden Formation (Fig. 2C; Drewes, 1971b; Inman, 1987). Age control within the fluvial to alluvial fan deposits of the lower red, brown, and upper red conglomerate members of the Santa Rita Mountains and alluvial fan to lacustrine deposits of the conglomerate and upper shale members in the Huachuca Mountains does not exist.

Magmatism in the southwestern U.S. Cordillera began migrating eastward from the Sierra Nevada and Peninsular Ranges starting at ca. 80 Ma and is thought to mark the beginning of flat slab subduction associated with the Laramide orogenic event (Coney and Reynolds, 1977; Dickinson, 1989; Ducea, 2001; Constenius et al., 2003; Copeland et al., 2017). Widespread Late Cretaceous arc magmatism in southeastern Arizona consists of local caldera systems and granitic intrusions that are genetically similar and regionally equivalent (Coney and Reynolds, 1977; Lipman and Sawyer, 1985; Dickinson, 1989; Mizer, 2018). In general, andesitic,

rhyolitic, and dacitic volcanic rocks are interbedded with and conformably overlie the uppermost members of synorogenic deposits. In the Santa Rita Mountains, thin rhyolitic tuffs are interbedded with the upper red conglomerate member and are conformably overlain by andesite and intracaldera breccias of the Mount Fagan rhyolite (Drewes, 1971b; Hayes and Drewes, 1978; Lipman and Sawyer, 1985; Ferguson et al., 2001; Dickinson, 2003).

SEDIMENTOLOGY AND PROVENANCE

Methods

Facies Analysis

We measured stratigraphic sections of the Fort Crittenden Formation; three were along the east flank of the Santa Rita Mountains and one was along the west flank of the Huachuca Mountains (Fig. 3). Lithofacies assemblages are based on detailed sedimentary facies analysis within measured stratigraphic sections totaling ~2500 m of stratigraphic thickness in the Santa Rita Mountains and ~800 m in the Huachuca Mountains. Lithofacies were classified according to a modified version of the lithofacies codes from Miall (1978) and DeCelles et al. (1991) and are summarized in Table 1.

Conglomerate Clast Counts and Paleocurrent Analysis

Conglomerate clast count data were collected at 19 localities in the Santa Rita Mountains and five in the Huachuca Mountains. At each locality, individual clasts were counted and identified within a 100 × 100 cm grid that was shifted parallel to bedding within the strata until 100 clasts were identified at each locality. Clast count data are shown as pie charts within their corresponding stratigraphic sections (Fig. 6). Paleocurrent directions were determined from imbricated

conglomerate clasts by measuring 5–10 clasts per location. Imbrication measurements were tilt-corrected based on measurements of master bedding.

Lithofacies Assemblages

Facies Assemblage A: Gcm, Gch/i, Gct/St, Fsm (3-D Dunes, Channels, and Longitudinal Gravel Bars)

Clast-supported massive conglomerate (Gcm/i): Moderately sorted, sub-angular to rounded, pebble to cobble conglomerate beds are structureless and form beds that are between 1.5 m and 10 m thick (Fig. 4A). Gcm facies are laterally traceable for tens of meters and have apparent erosional bases. Fining upward trends within beds of Gcm are observed, although these are uncommon. Clast imbrication (Gcmi) is common with the long axis perpendicular to flow.

Clast-supported horizontally stratified conglomerate (Gch/i): Facies Gch is characterized by horizontally stratified, poorly sorted, sub-angular to rounded, pebble to cobble conglomerate units (Fig. 4B). Beds of Gch range from 1.5 m to 10 m in thickness, are laterally traceable for tens of meters, and have erosional bases. Cobble size clasts in Gch facies typically exceed 100 mm. Clast imbrication (Gchi) is common with the long axis perpendicular to flow.

Clast-supported trough cross-stratified conglomerate (Gct): Facies Gct consists of trough cross-stratified, moderately sorted, sub-rounded, pebble to cobble conglomerate beds that range from 0.25 m to 6 m in thickness. Gct intervals commonly have erosional bases (~1 m of relief) and fine upward to St facies (Fig. 4C).

Trough cross-stratified sandstone (St): Fine to very coarse-grained, trough cross-stratified sandstone are typically >2 m thick and are often wedged between or occur above Gct facies (Fig. 4C). St beds have erosional bases and fine

upwards. Gravel to pebble stringers are often incorporated with St facies at the base of troughs.

Massive siltstone (Fsm): Massive red siltstone beds range from 0.3 m to 6 m in thickness and typically cap beds of sandstone (Sm, Sh, St; Fig. 4D). Fsm facies are weakly calcareous with small nodules of calcium carbonate ~1 mm in diameter.

Interpretation: Conglomerate facies (Gcm/i, Gch/i, and Gct) result from deposition in gravely bedload channels (Nemec and Steel, 1984; Miall, 1985). Beds of Gct to St represent the migration of 3-D dune bedforms within channels (Miall, 1996). These facies are typical of sandy braided fluvial systems including fining upward cycles, high sand content, and vertically stacked channel deposits (Miall, 1977). Erosional bases and fining upward trends within conglomerate facies (Gcm, Gct, Gch) likely represent bed-load channel deposits and channel bars (Miall, 1977, 1985; Nemec and Steel, 1984). Gct to St facies are interpreted as migrating subaqueous 3-D dunes deposited within channels (Miall, 1996). Sandstone beds (St, Sm, Sh) and limited Fsm facies represent deposition in shallow braided channels under waning flow conditions (Miall, 1977; DeCelles et al., 1991). Thick sandstone beds represent vertical channel aggradation (Miall, 1977).

Facies Assemblage B: Gct/St, Sm/Fsl (Channel Bar Migration)

Clast-supported trough cross-stratified conglomerate (Gct): Gct facies as described in Facies Assemblage A are generally ~3 m in thickness (Fig. 4C). Inclined surfaces of Gct/St facies cut into interbedded Sm, Fsm, and Fsl facies.

Trough cross-stratified sandstone (St): Very coarse-grained, trough cross-stratified sandstone facies are 2 m thick and occur above Gct facies (Fig. 4C). Inclined surfaces of trough

TABLE 1. LITHOFACIES CODES AND INTERPRETATIONS USED IN THIS STUDY

Facies assemblage	Dominant lithofacies assemblage	Description	Stratigraphic occurrence	Interpretation
A	Gcm/i, Gch/i, Gct/St	Pebble-cobble, clast-supported, moderately sorted conglomerate; imbrication, horizontally stratified, trough cross-stratified, and massive.	Lower red conglomerate member; Brown conglomerate member	3-D dunes, channels, and longitudinal gravel bars; braided fluvial system
B	Gct/St, Sm/Fsl	Trough cross-stratified conglomerate and sandstone with high relief erosional bases; interbedded massive sandstone and laminated siltstone beds; Gct/St beds cut into Sm/Fsl beds.	Lower red conglomerate member	channel bar migration; braided fluvial system
C	Sh, Sm, Fsm	Horizontally stratified and massive sandstone beds 1 m to 5 m thick with erosional bases. Massive red siltstone cap sandstone beds.	Lower red conglomerate member; Brown conglomerate member	Channel deposits; braided fluvial system
D	Fsl, Fsm, Sm	Laminated and massive gray siltstone. Organic-rich horizons and calcium nodules occur but are uncommon; thin, massive, tabular sandstone beds are interbedded with siltstone beds.	Brown conglomerate member	Overbank and crevasse splay deposits; braided fluvial system
E	Gcm, Gch, Gct, Sm/St	Pebble to boulder, clast-supported, poorly sorted, subangular to rounded conglomerate; laterally extensive trough cross-stratified and massive sandstone beds; lenticular and sheet-like geometries observed.	Upper red conglomerate member; Conglomerate member	Sheetflood alluvial-fan; streamflow alluvial fan
F	Sm/Fsm, St/Sh	Interbedded, laterally extensive, massive sandstone and siltstone/shale beds; siltstone/shale contain gastropods.	Upper shale member	Freshwater lacustrine deposits

Note: Modified after Miall (1978) and DeCelles et al. (1991).

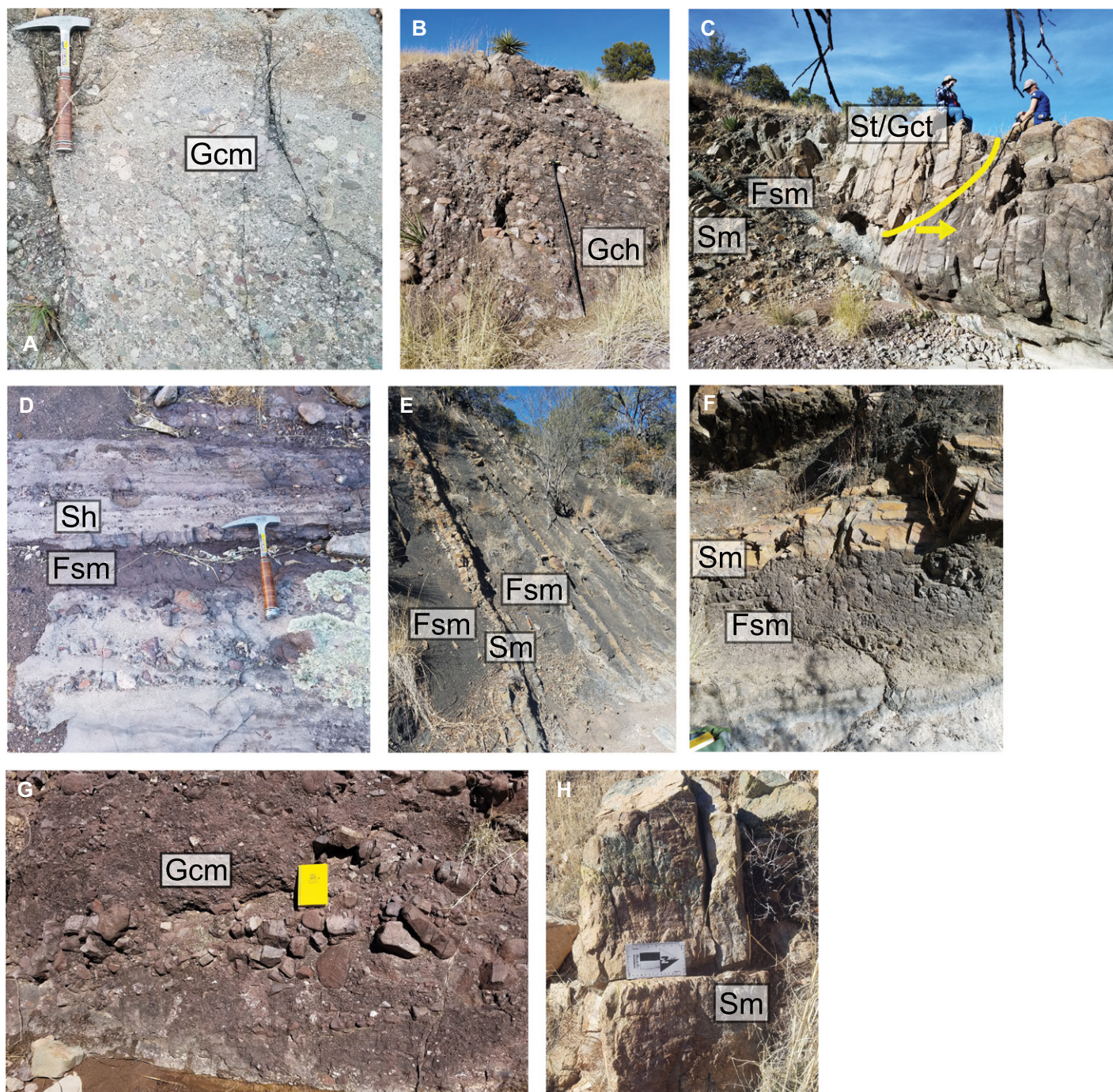


Figure 4. Photographs show common lithofacies of the Fort Crittenden Formation in the Santa Rita Mountains in the (A–E) lower red conglomerate, (F) brown conglomerate, and (G and H) upper red conglomerate members. See Table 1 for lithofacies description and interpretation. Lithofacies descriptions: Fsm—massive siltstone or paleosol; Sm—massive sandstone; Sh—horizontally bedded sandstone; St—trough cross-bedded sandstone; Sh—horizontally bedded sandstone; Gcm—massive clast-supported conglomerate; Gch—horizontally bedded, clast-supported conglomerate; and Gct—trough cross-bedded, clast-supported conglomerate.

cross-stratified St sandstone, associated with Gct facies, cut into interbedded Sm, Fsm, and Fsl facies. St beds have erosional bases and fine upwards.

Massive sandstone (Sm): Massive fine-grained sandstone form thin beds up to 1 m

thick and are commonly interbedded with Fsm and Fsl facies. Beds of Sm facies can be traced laterally for tens of meters (Figs. 4C and 4E).

Laminated siltstone (Fsl): Laminated black to gray siltstone forms beds up to 0.25 m thick that are not commonly observed. Bivalves are

common in Fsl facies beds. Thin (<0.25 m), very fine- to fine-grained sandstone beds (Sm) are interbedded within Fsl facies. Light to dark gray siltstone beds range from 0.3 m to 6 m in thickness and typically cap thin, fine-grained beds of sandstone (Sm).

Interpretation: Lateral accretion surfaces and interbedded Fsl and Sm facies were only observed once throughout the lower red conglomerate section (Fig. 4C). Lateral accretion surfaces indicate either migration of channel bars or lateral accretion on a point-bar (Miall, 1977). Based on the one-time occurrence of Fsl and Sm facies with lateral accretion surfaces and lack of overbank deposits, we interpret this facies assemblage to represent migration of channel bars in ephemeral braided streams (Miall, 1977; Cant and Walker, 1978; Lunt et al., 2004).

Facies Assemblage C: Sh, Sm, Fsm (Channel)

Horizontally stratified sandstone (Sh): Fine- to medium-grained, horizontally stratified sandstone is commonly associated with Gch, Gcm, and Fsm facies. Sh beds range from 0.5 m to 1 m in thickness and typically have erosional bases. Normal grading is apparent in Sh facies but is uncommon. Strings of gravel and pebbles are common at the base Sh beds (Fig. 4D).

Massive sandstone (Sm): Massive fine- to very coarse-grained sandstone form beds ranging from 0.5 m to 5 m in thickness. Fining upward trends are apparent within beds of Sm intervals thicker than 1 m.

Massive siltstone (Fsm): Light to dark gray siltstone beds range from 0.3 m to 6 m in thickness and typically cap thin, fine-grained beds of sandstone (Sm). Fsm beds are laterally extensive for tens of meters and have an erosional base. Organic-rich horizons and calcium carbonate nodules occur but are uncommon (Fig. 4D).

Interpretation: Sandstone facies (St, Sh, Sm) represent waning flow conditions within braided channels (Bluck, 1964; Rasmussen, 2000). Red Fsm intervals capping bodies of sandstone and conglomerate were deposited under waning flow conditions and later modified by pedogenesis. Overall, Facies Assemblages A through C represent deposition in a sandy-gravelly braided fluvial system. This interpretation is supported by dominant conglomeratic bed-load and sandstone channel deposits that exhibit large-scale fining upward trends and the general lack of lateral accretion surfaces and overbank deposits (Miall, 1977; DeCelles et al., 1991).

Facies Assemblage D: Sm, Fsl, Fsm (Overbank and Crevasse Splay)

Massive sandstone (Sm): Thin, tabular, massive fine-grained sandstone beds are <1 m thick and can be traced laterally for tens of meters (Fig. 4F). Thin intervals of Sm commonly alternate with beds of Fsm.

Laminated siltstone (Fsl): Thick beds of Fsl facies (>0.5 m) are as described in Facies

Assemblage C and are laminated. Thin (<0.5 m), very fine- to fine-grained sandstone beds (Sm) are interbedded with Fsl and Fsm facies. Bivalves are common in thin Fsl facies beds.

Massive siltstone (Fsm): Fsm facies, as described in Facies Assemblage C, are laterally extensive for tens of meters and have erosional bases. Organic-rich horizons and calcium carbonate nodules occur but are uncommon (Fig. 4F). Thin, laterally extensive Sm facies with erosional bases are interbedded with Sm, Fsl, and Fsm layers.

Interpretation: Fine-grained, laminated beds of Fsl are interpreted as overbank deposits. Thin, tabular beds of Sm facies interbedded with overbank facies (Fsl) are interpreted as crevasse-splay deposits (DeCelles et al., 1991). Dark gray Fsm facies are interpreted as well-developed paleosols, most likely gleysols, based on the organic-rich horizons and calcium nodules (Mack, 1993; Tabor et al., 2008; Thomas et al., 2011). The presence of gleysols indicates reducing conditions and periodically water-saturated environments such as a fluvial floodplain (Tabor et al., 2008).

Facies Assemblage E: Gcm, Gch, Gct, Sm/St (Alluvial Fan)

Clast-supported massive conglomerate (Gcm): Moderately to poorly sorted, sub-angular pebble to boulder conglomerate beds are structureless and form beds between 1 m and 25+ m thick (Figs. 4G and 5A). Gcm beds do not consistently exhibit fining upward trends, have apparent erosional bases, and are laterally extensive for tens of meters. Lenticular bodies of Gcm facies are 1–3 m thick and are encased in Sm and St facies. Clast imbrication (Gcmi) is observed with the long axis perpendicular to flow, although this is uncommon.

Clast-supported horizontally stratified conglomerate (Gch): Poorly sorted, sub-angular pebble to boulder conglomerate beds are horizontally stratified and range from 1 m to 25+ m in thickness. Individual beds are traceable for tens of meters and have apparent erosional bases. Lenticular bodies of Gch facies are 1–2 m thick and are encased in Sm and St facies. Clast imbrication (Gchi) is observed with the long axis perpendicular to flow, although this is uncommon. Fining upward trends within beds of Gch are observed and are common.

Clast-supported trough cross-stratified conglomerate (Gct): Moderately sorted sub-angular pebble to cobble conglomerate form trough cross-stratified beds up to 10 m in thickness. Beds of Gct are laterally extensive for tens of meters and fine upward to St facies. Gct facies are uncommon in Facies Assemblage D. Lenticular bodies of Gct facies are

1–2 m thick and are encased in Sm and St facies (Fig. 5B).

Massive sandstone (Sm): Fine- to coarse-grained beds of massive sandstone range from 1 m to >10 m in thickness and occur as laterally extensive tabular bodies (Fig. 4H). Lenticular bodies of Sm facies are ~1 m thick and are encased by Gcm and Gch facies. Fining upward trends within intervals of Sm occur but are not consistently observed. Gravel to pebble stringers are often incorporated with Sm facies.

Trough cross-stratified sandstone (St): Fine- to medium-grained trough cross-stratified beds of sandstone range from 3 m to >10 m in thickness. The lateral extent of St facies is not clear due to outcrop quality, and these beds often have erosional bases or occur above Gct facies. St beds fine upward and contain gravel to pebble stringers that are often incorporated with St facies at the base of troughs.

Interpretation: Facies Assemblage E is interpreted to represent streamflow and sheetflood-dominated alluvial fan deposits. Evidence of streamflow depositional processes includes massive to horizontally stratified, well-sorted, and lenticular conglomerate beds. These features indicate deposition under bedload conditions and are interpreted as longitudinal bars (Ridgway and DeCelles, 1993; Rasmussen, 2000). Evidence of sheetflood depositional processes includes horizontally stratified, poorly-sorted, sub-angular, and laterally extensive conglomerate beds. Large-scale, fining upward trends observed between conglomerate and sandstone beds indicate waning flow conditions (Allen et al., 1981; Mack and Rasmussen, 1984). Facies Assemblage E, coupled with the lateral extent and predominance of Gcm facies and complete absence of fine-grained facies, suggest deposition in the medial part of an alluvial fan. This interpretation is consistent with the predominance of this facies assemblage at the top of the Fort Crittenden Formation section in the Santa Rita Mountains, the overall coarsening upward trend, and the paleodrainage evolution discussed below.

Facies Assemblage F: Sm/Fsm, St/Sh (Lake)

Massive sandstone (Sm): Massive fine- to medium-grained beds of Sm facies are laterally extensive and occur in beds <2 m thick. Sm beds are either associated with St and Sh facies or are interbedded with Fsm facies (Fig. 5D).

Horizontally stratified sandstone (Sh): Fine-grained, horizontally stratified beds of Sh occur in beds that are <2 m thick and laterally extensive. Limited Sh beds occur above St and Sm facies.

Trough cross-stratified sandstone (St): Fine- to medium-grained, trough cross-stratified sandstone beds are tabular and laterally extensive for tens of meters (Fig. 5C). St facies are

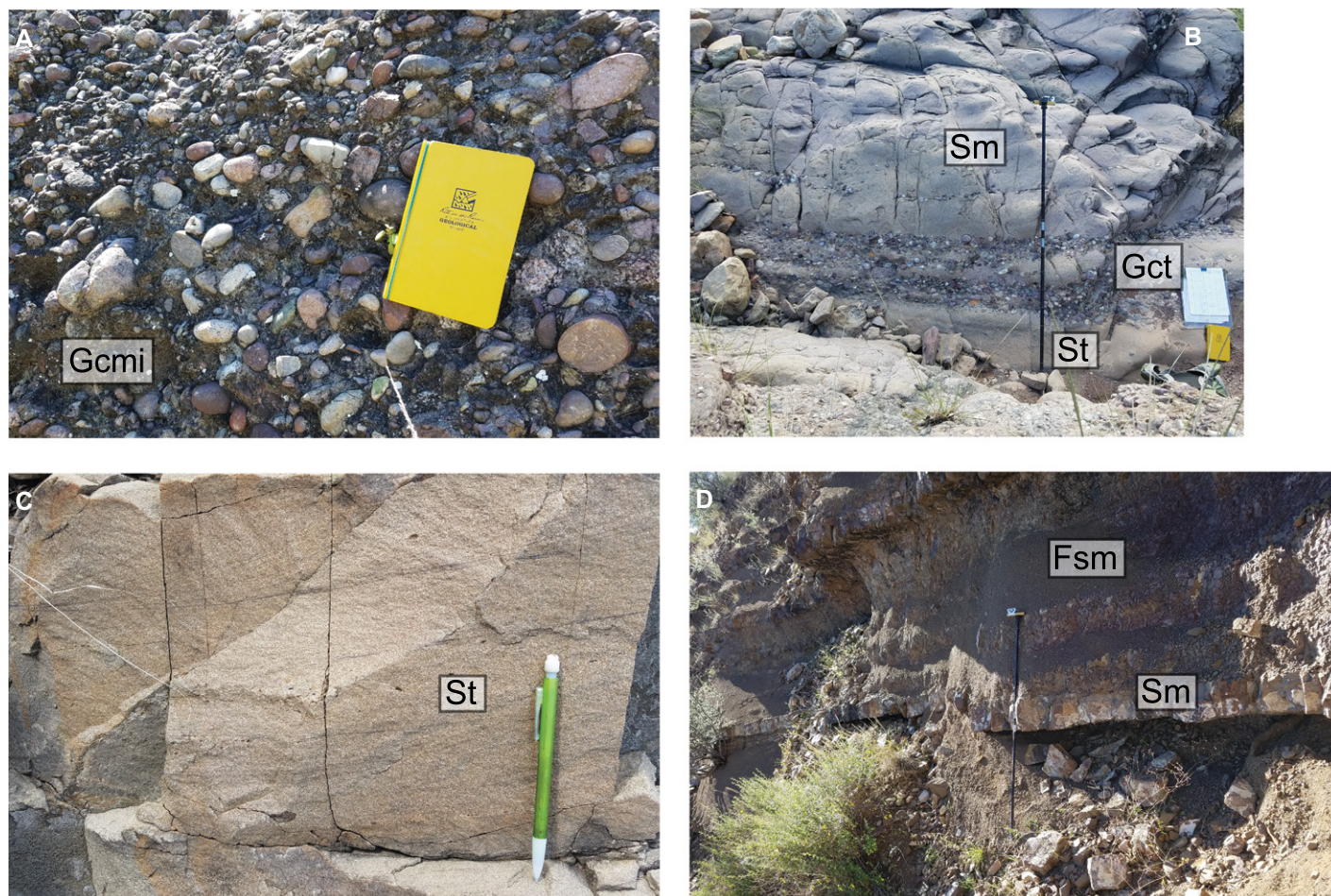


Figure 5. Photographs show common lithofacies of the Fort Crittenden Formation in the Huachuca Mountains in the (A–B) conglomerate member and the (C–D) upper shale member. See Table 1 for lithofacies description and interpretation. Lithofacies descriptions: Fsm—massive siltstone or paleosol; Sm—massive sandstone; Sh—horizontally bedded sandstone; St—trough cross-bedded sandstone; Sh—horizontally bedded sandstone; Gcmi—massive clast-supported imbricated conglomerate; Gch—horizontally bedded, clast-supported conglomerate; and Gct—trough cross-bedded, clast-supported conglomerate.

typically <3 m in thickness and rarely contain gravel and pebbles in troughs.

Massive siltstone to paleosol (Fsm): Massive gray beds of Fsm consist of siltstone and shale deposits that are laterally extensive for tens of meters and are interbedded with sandstone facies (Fig. 5D). Dark gray shale beds of Fsm often contain freshwater gastropods.

Interpretation: Facies Assemblage F consists entirely of interbedded sandstone and siltstone/shale facies. Dark gray shale and siltstone beds lack evidence of pedogenic modification and suggest that these deposits are not characteristic of a floodplain. Gastropods and mollusks in gray shale and siltstone beds have been interpreted to indicate freshwater lacustrine deposition (Hayes, 1970b). Coarsening upward sandstone to fine-grained intervals indicate progradation of a fluvial system into lacustrine environments (Ridgway and DeCelles, 1993).

Stratigraphic Distribution of Lithofacies Assemblages

The lower red conglomerate member (Fig. 6A) is mainly characterized by facies Gcm, Gch/i, Gct/St and Sh, Sm, Fsm (Table 1), typical of Facies Assemblages A and C, which indicates deposition by channels, 3-D subaqueous dunes, and longitudinal gravel bars in a braided fluvial system. Facies Assemblage B (Gct/St, Sm/Fsl) is observed once at ~50 m from the base of the lower red conglomerate measured section and indicates channel bar migration (Fig. 4C). The remaining ~900 m of measured section is characterized by Facies Assemblages A and C.

The brown conglomerate member (Fig. 6B) is characterized by facies Gcm, Gch/i, Gct/St and Sh, Sm, Fsm (Table 1), typical of Facies Assemblages A and C, which indicates deposition by 3-D subaqueous dunes, channels, and longitudinal gravel bars in a sandy braided

fluvial system (Fig. 4A). At ~450 m, a thick intrusive layer (hypabyssal) is present in the brown conglomerate in the Santa Rita Mountains (Fig. 6B). Facies Assemblage D (Fsl, Fsm, Sm) is observed between 800 m and 1000 m in the brown conglomerate section and indicates overbank and crevasse splay deposition in overbank areas within a braided fluvial system (Fig. 4F).

The upper red conglomerate member in the Santa Rita Mountains (Fig. 6C) and the conglomerate member in the Huachuca Mountains (Fig. 6D) are characterized by facies Gcm, Gch, Gct and Sm/St (Table 1), typical of Facies Assemblage E, which indicates alluvial fan deposition. Sheet-like geometries of the alluvial fan deposits of the upper red conglomerate member indicate sheetflood deposition (Figs. 4G and 4H). Lenticular geometries of deposits of the conglomerate member suggest streamflow deposition (Figs. 5A–5B).

Conglomerate Clast Counts and Paleocurrent Analysis

Results

Conglomerate clasts from the lower red conglomerate member are predominantly composed of rhyolitic (40%), granitic (25%), quartzite (17%), and andesitic (15%) clasts. The abundance of volcanic clasts increases up-section in the lower red conglomerate member (Fig. 6A). Paleocurrents measured from the lower red conglomerate indicate that the detritus was deposited in a northeastward-flowing system (Fig. 6A). Clasts from the brown conglomerate member contain varying amounts of volcanic, granitic, and siltstone clasts and minor amounts of sandstone and quartzite clasts. Paleocurrent measurements were not available from the brown conglomerate. The number of siltstone clasts increases up-section from 13% to 33% (Fig. 6B). Conglomerate clast compositions from the upper red conglomerate member consist mainly of recycled sedimentary and siltstone (75%) clasts and minor amounts of rhyolite and quartzite clasts (Fig. 6C). Paleocurrent data from the upper red conglomerate indicate southwestern sediment transport (Fig. 6C).

In the Huachuca Mountains, the conglomerate member consists of subequal amounts of granitic, rhyolitic, and siltstone clasts and minor amounts of andesitic clasts. There are no distinct trends in clast lithologies observed within the conglomerate member (Fig. 6D). Paleocurrent measurements in the conglomerate member are limited in both this study and that of Hayes (1986) and suggest a south to southwest paleocurrent direction.

Interpretation

Paleocurrent measurements and conglomerate clast compositions from the lower red and brown conglomerate members indicate that these deposits were largely derived from rhyolitic, andesitic, and granitic sources in a northeast-flowing depositional system (Figs. 6A–6B). Quartzite clasts, observed mostly in the lower red conglomerate, were likely derived from the Bolsa Quartzite, although no present-day exposures are located southwest of the Santa Rita Mountains. Igneous clast lithologies are consistent with local exposures of Jurassic igneous rocks and Proterozoic continental granodiorite located southwest of the Santa Rita Mountains (Drewes, 1971a). The upper red conglomerate member records a shift in paleodrainage and sediment source. Increased amounts of recycled sedimentary clasts possibly reflect input from sandstone and siltstone lithologies that make up the uppermost member of the Bisbee Group, the

Cintura Formation that is exposed to the northeast of the upper red conglomerate member. This interpretation is supported by a southwest paleoflow.

Conglomerate clast composition and paleocurrent measurements from the conglomerate member in the Huachuca Mountains indicate a mixed sediment source derived primarily from granitic, rhyolitic, and siltstone sources located north to northeast of the Huachuca Mountains (Fig. 6D). These results are consistent with local exposures of the Proterozoic continental diorite, unnamed siliceous volcanic rocks, and Canelo Hills volcanic rocks. Siltstone clasts may reflect input from Paleozoic sedimentary rocks and/or Cambrian sedimentary rock sources.

Conglomeratic facies and paleocurrent measurements from the lower red and brown conglomerate members in the Santa Rita Mountains indicate deposition in a northeastward-flowing braided fluvial system. These members were primarily supplied by local uplifts of Jurassic granitic and volcanic rocks located southwest of the study area. A marked shift in depositional environment, paleodrainage, and clast composition are recorded with deposition of the upper red conglomerate member, which indicates southwestward-flowing, sheetflood-dominated alluvial fan deposition possibly supplied by the Bisbee Group to the northeast. The Fort Crittenden Formation in the Huachuca Mountains records deposition by braided streams and stream-dominated alluvial fans flowing south to southwestward. These deposits were primarily derived from local volcanic sources, Paleozoic sedimentary rocks, and Proterozoic continental granodiorite located north of the study area (Hayes, 1986; and this study).

DETRITAL ZIRCON U-Pb GEOCHRONOLOGY

U-Pb detrital zircon geochronology is used in this study to: (1) determine the provenance of the Fort Crittenden Formation; and (2) constrain a maximum depositional age of the Fort Crittenden Formation (Dickinson and Gehrels, 2009). Zircons were separated using standard mineral separation procedures in use at the Arizona LaserChron Center, mounted in epoxy with grains of standards SL2 (563.2 ± 4.8 Ma; Gehrels et al., 2008), R33 (419.3 ± 0.4 Ma; Black et al., 2004), and FC-1 (1099.5 ± 0.33 Ma; Paces and Miller, 1993), polished to a depth of ca. 20 μm , and a series of back-scattered electron images (BSE) and/or cathodoluminescence images (CL) were acquired using a Scanning Electron Microscope (SEM) before laser ablation.

U-Pb data for this study were collected by laser ablation-inductively coupled plasma-mass spectrometry (LA-ICP-MS) at the University of Arizona LaserChron Center using methods described in Pullen et al. (2018). Analyzed grains were ablated using a Photon Machines Analyte G2 excimer laser coupled to an Element2 HR ICP-MS that sequences through U, Th, Pb, and Hg isotopes. A total of 315 randomly selected detrital grains were analyzed for each sample at a spot size of 20 μm . Uncertainties reported for individual analyses include random uncertainty of the measured $^{206}\text{Pb}/^{238}\text{U}$ and $^{204}\text{Pb}/^{206}\text{Pb}$ as well as any overdispersion factor (Horstwood et al., 2016). Random and systematic uncertainties for weighted mean ages are calculated as the quadratic sum of the weighted mean uncertainty. Random uncertainties are calculated based on the dispersion of individual analyses, whereas systematic uncertainty includes uncertainties associated with the age of zircon standards, the decay constants, the session fractionation correction, and the common Pb correction.

Methods

U-Pb Geochronology

Zircons from seven ~ 10 kg medium- to coarse-grained sandstone samples of the Fort Crittenden Formation were analyzed for detrital zircon ages using LA-ICP-MS geochronology to calculate maximum depositional ages (MDA) and assess sediment provenance. In the Santa Rita Mountains, samples were collected at the base and top of the lower red conglomerate (FC-AC18-1 and FC-AC18-4) and upper red conglomerate (FC-HC18-1 and FC-HC18-2) members and in the middle of the brown conglomerate member (FC-CC18-1; Fig. 3B). In the Huachuca Mountains, sandstone samples were collected at the base and top of the Fort Crittenden Formation (FC-BCY18-1 and FC-BCY18-2) (Fig. 3C). Potential sediment source samples were selected based on igneous conglomerate clast lithologies observed and paleocurrent measurements in the lower red and brown conglomerate members. Samples include Comoro Canyon granite from south of the Santa Rita Mountains and from the Proterozoic Continental Granodiorite exposed along the west flank of the Santa Rita Mountains (Fig. 3A). Detrital zircon sample locations from the study are reported in Table 2.

A total of 2142 detrital zircon ages are reported in Figure 7 and the supplemental document. Random uncertainties for individual grains are reported at 1σ level. Reported ages younger than 1000 Ma are $^{206}\text{Pb}/^{238}\text{U}$ and reported ages older than 1000 Ma are $^{206}\text{Pb}/^{207}\text{Pb}$ ages. The following filters were applied to the reduced data where individual analyses were rejected if

TABLE 2. LOCATIONS FOR SAMPLES FROM THIS STUDY

Sample no.	Area	Lithology	Analysis	Latitude (°N)	Longitude (°W)
FC-AC18-1	Santa Rita Mts.	Lower red conglomerate Fort Crittenden Fm. Sandstone	Detrital zircon	31.687687	-110.770768
FC-AC18-4	Santa Rita Mts.	Lower red conglomerate Fort Crittenden Fm. Sandstone	Detrital zircon	31.694284	-110.765636
FC-CC18-1	Santa Rita Mts.	Brown conglomerate Fort Crittenden Fm. Sandstone	Detrital zircon	31.718235	-110.777570
FC-HC18-1	Santa Rita Mts.	Upper red conglomerate Fort Crittenden Fm. Sandstone	Detrital zircon	31.703904	-110.762742
FC-HC18-2	Santa Rita Mts.	Upper red conglomerate Fort Crittenden Fm. Sandstone	Detrital zircon	31.705426	-110.761000
FC-BCY18-1	Huachuca Mts.	Conglomerate member Fort Crittenden Fm. Sandstone	Detrital zircon	31.511284	-110.462597
FC-BCY18-2	Huachuca Mts.	Upper shale member Fort Crittenden Fm. Sandstone	Detrital zircon	31.515009	-110.472603
FC-AC17-7	Santa Rita Mts.	Fort Crittenden Fm. granitic clast	AFT/AHe	31.688480	-110.770130
FC-AC18-2B	Santa Rita Mts.	Fort Crittenden Fm. granitic clast	AFT	31.690073	-110.767622
MW18-3	Santa Rita Mts.	Josephine Cnyn. Diorite	AFT	31.696805	-110.863626
MW18-4	Santa Rita Mts.	Madera Cnyn. Granodiorite	AFT	31.708850	-110.870650
JG-18	Santa Rita Mts.	Comoro Cnyn. Granite	U-Pb	31.391776	-110.880880
PG-18-1	Santa Rita Mts.	Proterozoic Continental Granodiorite	U-Pb	31.781175	-110.828928
SF-MF-1	Santa Rita Mts.	Salero Formation andesite	U-Pb and Lu-Hf	31.902560	-110.696500
SF-MF-2	Santa Rita Mts.	Salero Formation dacite	U-Pb and Lu-Hf	31.896999	-110.694010
SF-RJ-1	Santa Rita Mts.	Salero Formation rhyolite	U-Pb and Lu-Hf	31.837420	-110.728900
FC-CC18-3	Santa Rita Mts.	Late Cretaceous intrusion	U-Pb and Lu-Hf	31.717183	-110.784133

Note: AFT—apatite fission track; AHe—apatite (U-Th)/He.

they met the following criteria: ages >1000 Ma with discordance >20%, analyses with reverse discordance >5%, and analyses with high ^{204}Pb (>600 cps). Ages that met these criteria were not considered in this study.

Maximum Depositional Ages

The maximum depositional age (MDA) of the Fort Crittenden Formation in the Santa Rita Mountains was calculated using four different methods run in Isoplot (Ludwig, 2008) on the uppermost sample from the upper red conglomerate member. MDA was not calculated using samples from the Huachuca Mountains due to a lack of grains <100 Ma.

The methods for calculating MDA include: (1) youngest graphical peak of a Probability Density Plot; (2) the Unmix age routine; (3) weighted mean; and (4) TuffZirc age routine. Grains between <113 Ma and >66 Ma were considered for these calculations. MDA calculated using these methods are reported in Table S1¹.

¹Supplemental Material. Maximum depositional ages, Lu-Hf, AFT, AHe, U-Pb ages, and detrital zircon U-Pb data. Please visit geochron.org to access new detrital zircon U-Pb geochronologic data. Please visit <https://doi.org/10.1130/GSAB.S.13289291> to access the supplemental material, and contact editing@geosociety.org with any questions.

Multidimensional Scaling

Multidimensional scaling (MDS) is an increasingly common statistical tool applied to quantify and visualize intersample dissimilarity in an N-dimensional Cartesian space (Vermesch, 2013). We implemented MDS using the program DZmds of Saylor et al. (2018). We used the Cross-correlation coefficient metric to quantify sample dissimilarity (Fig. 8). The Cross-correlation coefficient uses the R^2 value of the cross-plot to assess intersample similarity and is sensitive to the presence/absence of age peaks and magnitude/shape of peaks (Saylor and Sundell, 2016). Samples that do not share age peaks and are

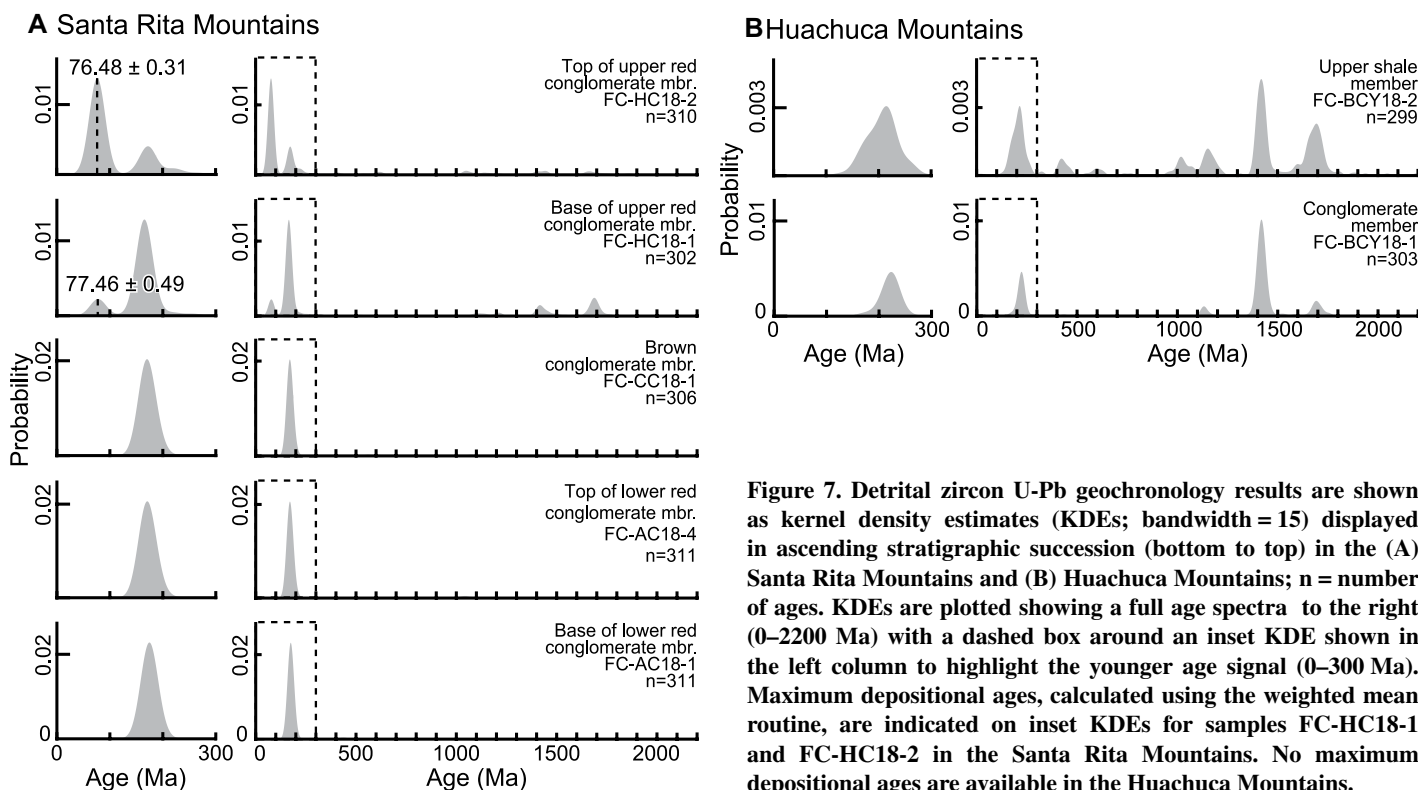


Figure 7. Detrital zircon U-Pb geochronology results are shown as kernel density estimates (KDEs; bandwidth = 15) displayed in ascending stratigraphic succession (bottom to top) in the (A) Santa Rita Mountains and (B) Huachuca Mountains; n = number of ages. KDEs are plotted showing a full age spectra to the right (0–2200 Ma) with a dashed box around an inset KDE shown in the left column to highlight the younger age signal (0–300 Ma). Maximum depositional ages, calculated using the weighted mean routine, are indicated on inset KDEs for samples FC-HC18-1 and FC-HC18-2 in the Santa Rita Mountains. No maximum depositional ages are available in the Huachuca Mountains.

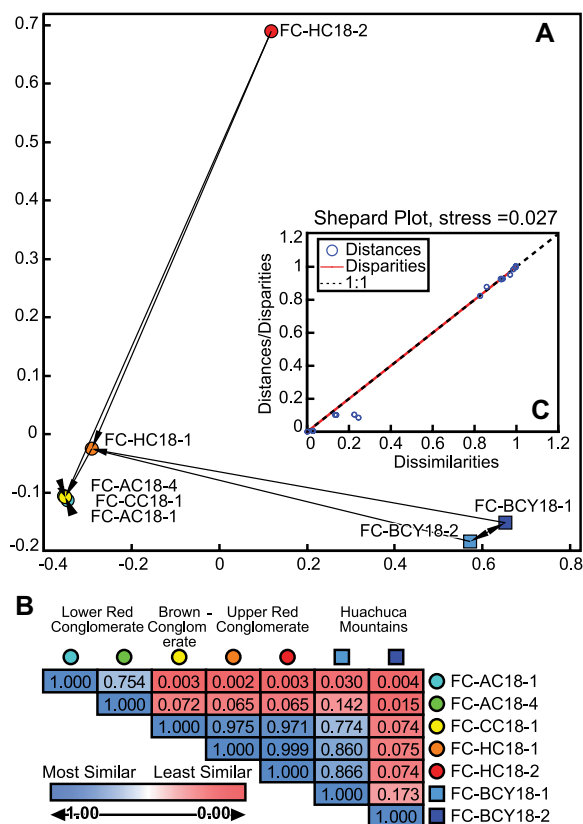


Figure 8. (A) Two-dimensional (2-D) multidimensional scaling (MDS) results of detrital zircon samples calculated using the (B) pairwise dissimilarity matrix. Black arrows on MDS plot indicate sample's nearest neighbor. (C) Shepard plot shows transformation from dissimilarity to distances and disparities. The low stress level of 0.027 indicates a reasonable transformation using the component of the Cross-correlation coefficient. Circles indicate samples of the Fort Crittenden Formation from the Santa Rita Mountains ($n = 5$), and squares indicate samples from the Huachuca Mountains ($n = 2$). Samples FC-AC18-1, FC-AC18-4, and FC-CC18-1 cluster close together, which indicates similar sediment sources. Samples in the upper red conglomerate, FC-HC18-1 and FC-HC18-2, plot increasingly farther away from the lower red and brown conglomerate cluster of samples due to changing sediment source. Samples FC-BCY18-1 and FC-BCY18-2 plot near each other, which indicates similar and locally derived sediment sources at the base and top of the Fort Crittenden Formation in the Huachuca Mountains.

dissimilar will result in a cross-correlation coefficient (R^2) that approaches 0. Increasingly, similar samples will result in an R^2 value that approaches 1.

Samples from the Fort Crittenden Formation ($N = 7$) are depicted by points on a 2-D MDS plot (Fig. 8A). Metric MDS converts a pairwise dissimilarity matrix (Fig. 8B) calculated from detrital zircon age distributions through iterative rearrangement of dissimilarities into N -dimension Cartesian space. The goal of MDS is to minimize the misfit between intersample calculated distances and the disparities; this is termed "stress" and is indicated by a Shepard plot (Fig. 8C). Stress indicates the correlation between sample dissimilarity and distance (misfit) and how reasonable a transformation is. A low-stress plot (0.025) indicates that the transformation is reasonable and that distances between points linearly correlate with intersample dissimilarities (Saylor et al., 2018). On the MDS plot, intersample dissimilarity is expressed as the distance among samples on the MDS plot (Fig. 8A). The greater the distance between points, the greater the sample dissimilarity.

Results

U-Pb Age Distribution—Santa Rita Mountains

Sandstone samples from the Fort Crittenden Formation in the Santa Rita Mountains are dominated by <200 Ma grains. A major age mode between ca. 160 Ma and ca. 175 Ma is present in each sample. A Campanian age mode at ca. 76 Ma is observed in both samples from the upper red conglomerate member (FC-HC18-1 and FC-HC18-2). Samples from the Santa Rita Mountains are composed of minor fractions of >200 Ma grains.

Detrital zircon age distributions from samples FC-AC18-1, FC-AC18-4, and FC-CC18-1 from the lower red and brown conglomerate members (0–900 m and 900–1900 m; Fig. 7A) are most similar. Dominant age modes in these three samples are between ca. 145 Ma and ca. 200 Ma and consistently decrease going up-section (Fig. 7A). At the base of the lower conglomerate member, 5% of the analyzed grains are older than ca. 200 Ma. At the top, 11% of analyzed grains are >200 Ma. The number of grains >200 Ma

increases from 5% to 11% going upwards in succession.

Samples from the base and top of the upper red conglomerate member of the Fort Crittenden Formation (FC-HC18-1 and FC-HC18-2) exhibit two age modes <200 Ma, at ca. 76 Ma and between ca. 164 Ma and ca. 174 Ma. The detrital zircon age distribution of sample FC-HC18-1 at the base of this member is composed of 50% of grains ca. 164 Ma and 10% of grains ca. 76 Ma (Fig. 7A). These proportions are reversed in sample FC-HC18-2 at the top of the upper red conglomerate member, where 47% of the sample records ages at ca. 76 Ma and 15% of ages at ca. 174 Ma. The remaining 30–40% of ages in both samples are <200 Ma.

Two basement samples were collected in the Santa Rita Mountains to compare against detrital zircon ages; one sample was collected from the Jurassic Comoro Canyon Granite south of the Santa Rita Mountains and the other from Proterozoic Continental Granodiorite exposed locally (Fig. 3A). These yielded weighted mean ages of 171.9 ± 3.37 Ma and 1434.5 ± 38.01 Ma respectively (Fig. S2; see footnote 1).

U-Pb Age Distribution—Huachuca Mountains

Both sandstone samples from the top and bottom of the measured Fort Crittenden Formation in the Huachuca Mountains are dominated by grains >500 Ma with fewer than 30% of grains younger than ca. 500 Ma (Fig. 7B). Detrital zircon ages in these two samples are similar in age groups but differ in proportionality. Proterozoic age grains compose $>70\%$ of measured ages in the sandstones sampled in the Huachuca Mountains with prominent age modes at ca. 1430 Ma and ca. 1700 Ma and smaller modes at ca. 1030 Ma and ca. 1150 Ma. Both samples exhibit significant Triassic through Jurassic age modes between ca. 180 Ma and ca. 225 Ma.

Maximum Depositional Ages

The Fort Crittenden Formation in the Santa Rita Mountains was previously estimated to be Santonian to Maastrichtian in age based on biostratigraphic, overlying chronostratigraphic, and lithostratigraphic age constraints (Miller, 1964; Drewes, 1971b; Hayes, 1986; Inman, 1987; Dalman et al., 2018). Maximum depositional ages were calculated using detrital zircon ages between <113 Ma and >70 Ma. Two samples in the Fort Crittenden Formation in the Santa Rita Mountains yielded grains with ages suitable for MDA calculation. These samples are from the base (FC-HC18-1) and top (FC-HC18-2) of the upper red conglomerate member. The weighted mean, TuffZirc, and Unmix age routines all provide

ages that are within uncertainty of each other and overlap with the youngest graphical peak MDA and are reported in Table S1. We report an MDA of ca. 77 Ma at the base of the upper red conglomerate member and 76 Ma at the top of the upper red conglomerate member (Fig. 7A).

Multidimensional Scaling

Detrital zircon samples from the Fort Crittenden Formation were compared using non-metric, two-dimensional, multidimensional scaling (MDS). The Shepard plot indicates a low stress and therefore an excellent fit for the nonmetric MDS ($S = 0.027$; Fig. 8C). The pairwise dissimilarity matrix used to construct MDS plots is color-coded to indicate similarity between age distributions (Fig. 8B is most similar and blue). Results show that Fort Crittenden Formation samples in the Santa Rita Mountains are dissimilar from samples in the Huachuca Mountains. Detrital zircon samples from the lower red and brown conglomerate members cluster close together and are therefore most similar to each other, yet they are dissimilar from samples in the upper red conglomerate. Sample FC-HC18-1 at the base of the upper red conglomerate plots closer to the aforementioned sample cluster than sample FC-HC18-2 from the top of the upper red conglomerate. This sample plots the furthest from lower red and brown conglomerate samples. Samples in the upper red conglomerate are the most dissimilar as shown by greater distances from each other (Fig. 8A). Fort Crittenden Formation samples from the Huachuca Mountains plot far away from both the cluster of lower red and brown conglomerate samples and upper red conglomerate samples. This indicates high dissimilarity among these groups of samples (Fig. 8).

Provenance Interpretation

Santa Rita Mountains

Detrital zircon ages and MDS results from the lower red and brown conglomerate members indicate that these deposits were derived from very similar sources (Figs. 7A and 8). Detrital zircon ages suggest that these members were largely derived from Jurassic arc sources consistent with local exposures of Jurassic igneous rocks in the Santa Rita Mountains including the Mount Wrightson Formation, the Piper Gulch Monazite, and Squaw Gulch Granite (Drewes, 1971a). Proterozoic zircons (>70%) were likely derived from basement local exposures of Continental Granodiorite and the Bolsa Quartzite, which is characterized by grains between 1.0 Ga and 1.2 Ga (Gross

et al., 2000; Stewart et al., 2001). Ages from basement granodiorite of ca. 1435 Ma (Fig. S2) are consistent with subordinate Precambrian age peaks in the lower red and brown conglomerate members (Fig. 7). MDS results indicate that age spectra of the lower red and brown conglomerate members are nearly identical; however, there is a notable increase in portions of Proterozoic age grains in the brown conglomerate member (Fig. 7A).

Detrital zircon samples from the upper red conglomerate reflect diverse sediment sources including the Laramide magmatic arc, the Jurassic magmatic arc, and Proterozoic basement rocks (Fig. 7A). Late Cretaceous zircons are more abundant at the top of the upper red conglomerate than at the base and indicate increased input from early Laramide arc magmatism starting at ca. 80 Ma (Dickinson, 1989; Mizer, 2018). Jurassic arc-derived zircons, conversely, decrease up-section. Proterozoic ages in these samples reflect basement sources similar to those of the lower red conglomerate. However, due to increased amounts of Proterozoic age zircons, basement rocks alone cannot explain elevated amounts of zircons in this age population. An additional sediment source is needed to explain these observations. Increased Proterozoic ages in the upper red conglomerate are consistent with detrital zircon age modes in the uppermost Bisbee Group member, the Cintura Formation (Fig. 2; Dickinson et al., 2009). Dickinson et al. (2009) interpreted Cintura Formation sandstones to have been primarily derived from recycled Jurassic eolianites from the eastern Colorado Plateau based on similar Proterozoic and Paleozoic detrital zircon ages (Dickinson et al., 2009). Based on the abundant sandstone and siltstone clasts, a southwestern paleoflow, and detrital zircon ages, we interpret the upper red conglomerate member to have been primarily derived from the Cintura Formation.

Huachuca Mountains

Detrital zircon ages and MDS results from the conglomerate member and upper shale member in the Huachuca Mountains indicate that these deposits were derived from similar sources but with some variation in Proterozoic ages observed (Figs. 7B and 8). Triassic and Jurassic age zircons are consistent with derivation from exposures of Triassic and Jurassic arc-related rocks such as the Canelo Hills volcanic rocks and unnamed siliceous volcanic rocks located north-to-northeast of the Huachuca Mountains. Because the majority of measured detrital zircon ages (>70%) are between ca. 1430 Ma and ca. 1700 Ma, we suggest that the Fort Crittenden Formation in the Huachuca Mountains was primarily derived from local exposures of Pro-

terozoic basement rocks similar to those in the Santa Rita Mountains with lesser contribution from Triassic–Jurassic sources.

Detrital zircon samples from the Huachuca Mountains did not yield a statistically significant number ($n = 3$) of grains with ages between 113 Ma and 70 Ma. The lack of depositional age zircons suggests that the Fort Crittenden Formation in the Huachuca Mountains was deposited before active Laramide magmatism in the southeastern Arizona region ca. 80 Ma and after 100 Ma based on stratigraphic relationships between the underlying Cintura Formation and overlying Cenozoic gravels. This interpretation is supported by similar vertebrate and invertebrate fossils in the upper shale member in the Huachuca Mountains and lower shale member in the Santa Rita Mountains. These fossils were assigned a Santonian to Campanian age (Hayes, 1970a; Hayes, 1986).

U-Pb AND Lu-Hf OF POST-DEPOSITIONAL MAGMATISM

Methods

Three igneous rock samples were collected from the Salero Formation, located comfortably on top of the Fort Crittenden Formation in the Santa Rita Mountains, and one was collected from an intrusive body along the brown conglomerate measured section for combined U-Pb and Lu-Hf analyses of both rims and cores to study crustal evolution during a period of post-depositional magmatism (Fig. 3A).

Lu-Hf isotope geochemistry analysis was conducted following methods described by Gehrels and Pecha (2014) and Ibanez-Mejia et al. (2014). Analyses reported in this study were conducted by LA-ICP-MS at the Arizona LaserChron Center using a Nu Plasma HR multicollector ICP-MS coupled to a New Wave 193 HE laser and to a Photon Machines analyte G2 excimer laser. Laser run conditions for Lu-Hf analysis were similar to those described for U-Pb analysis. Three out of the four samples collected in this suite yielded zircons for combined U-Pb and Lu-Hf isotopic analyses. Hf analyses were conducted at a spot size of 40 μm diameter directly on top of previous U-Pb analysis pits of 20 μm diameter, with the exception of those that were too small, to allow Hf data to be directly tied to a U-Pb age. Zircon standards (FC, R33, Mud Tank, Temora-2, 91500, Plesovice, and SL2) were added to each sample mount and analyzed among unknown zircons. Lu-Hf isotopic results are reported at the 1σ level and as $\epsilon\text{Hf}(t)$, indicating the timing of zircon crystallization based on U-Pb geochronology results (Fig. 9; Vervoort and Patchett,

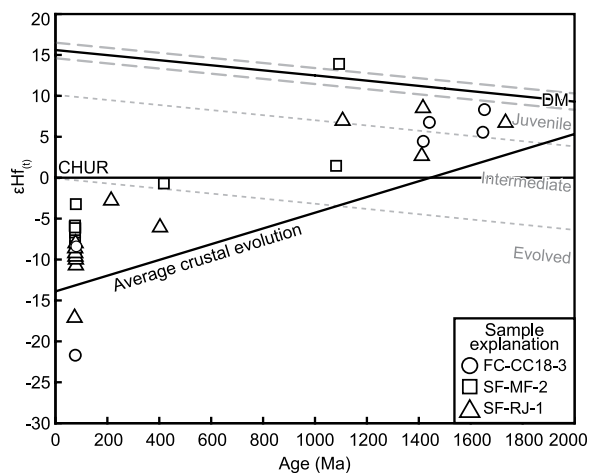


Figure 9. Combined U-Pb geochronology and $\epsilon\text{Hf}(t)$ isotopic results are shown for Late Cretaceous igneous rocks: the Salero Formation samples (SF-MF-2 and SF-RJ-1) and the Late Cretaceous intrusion sample (FC-CC18-3) in the Santa Rita Mountains ($n = 35$). Samples are plotted as different symbols. DM—depleted mantle; CHUR—chondritic uniform reservoir, average crustal evolution = 0.0115 (Vervoort and Patchett, 1996). Evolved $\epsilon\text{Hf}(t)$ values correspond with Late Cretaceous ages and intermediate-to-juvenile $\epsilon\text{Hf}(t)$ values correspond with inherited Proterozoic ages.

intermediate-to-juvenile $\epsilon\text{Hf}(t)$ values correspond with inherited Proterozoic ages.

1996). Sample locations from this study are reported in Table 2. Combined U-Pb and $\epsilon\text{Hf}(t)$ data are reported in the supplementary files. An average ratio for crustal evolution is assumed in this study: $^{176}\text{Lu}/^{177}\text{Hf} = 0.0115$ (Vervoort and Patchett, 1996).

Results

U-Pb Geochronology

Zircons from the four igneous lithologies yielded three crystallization ages and two distinct populations of inherited ages (Fig. 9). Crystallization ages for the dacite, rhyolite, and intrusion samples are between ca. 75 Ma and ca. 73 Ma and were calculated using the weighted mean and TuffZirc methods. The andesite sampled from the Salero Formation, SF-MF-1, produced a total of three zircons, and therefore no effective weighted mean age or TuffZirc calculated ages are reported for this sample.

Major age modes observed in the Salero Formation dacite and rhyolite and the intrusion samples are ca. 70 Ma to ca. 80 Ma, 1.4 Ga, and 1.6–1.7 Ga. The dacite sample, SF-MF-2, produced a total of 39 U-Pb ages exhibiting one major age peak between ca. 73 Ma and ca. 78 Ma. Sample SF-RJ-1 was collected from the Mount Fagan Rhyolite in the northern Santa Rita Mountains and produced 57 U-Pb ages.

Of the 57 ages, 80% fall between ca. 77 Ma and ca. 70 Ma, 5% result in peaks at 1.4 Ga and 1.6–1.7 Ga, and the remaining 15% are randomly distributed between ca. 90 Ma and ca. 1.07 Ga. The intrusion sample, FC-CC18-3, resulted in 31% of ages between ca. 74 Ma and ca. 78 Ma, 11% at 1.4 Ga, 24% at 1.6 Ga, and 9% at 1.7 Ga.

Hafnium Isotope Geochemistry

Combined U-Pb and Lu-Hf results are reported for three igneous rock samples in Fig-

ure 9 and in Table S2 (see footnote 1). A total of 35 new U-Pb ages with combined $\epsilon\text{Hf}(t)$ ranges for these samples are presented. The dacite and rhyolite samples from the Salero Formation are predominantly composed of ca. 80–70 Ma zircon ages that yield $\epsilon\text{Hf}(t)$ values between -10.8 and -3.2 and are secondarily composed of >1.0 Ga inherited zircon cores that yield $\epsilon\text{Hf}(t)$ values of $+1.4$ to $+8.5$. The rhyolite sample contains one outlying $\epsilon\text{Hf}(t)$ value in the 80–70 Ma age range of -17.1 . The intrusion sample yielded $\epsilon\text{Hf}(t)$ values between -8.4 and -6.4 for 80–70 Ma zircons, one outlying $\epsilon\text{Hf}(t)$ value of -21.7 in the 80–70 Ma range, and $\epsilon\text{Hf}(t)$ values between $+4.4$ and $+6.8$ for older zircons >1.0 Ga. Throughout all three samples, five analyses randomly scatter between ca. 800 Ma and 200 Ma and produced scattered $\epsilon\text{Hf}(t)$ values. We consider $\epsilon\text{Hf}(t)$ values ranging from $+10$ to $+15$ to be juvenile, 0 to $+10$ to be intermediate, and $\epsilon\text{Hf}(t) < 0$ to be evolved. Combined U-Pb- $\epsilon\text{Hf}(t)$ results fall into two distinct groups: (1) older inherited zircons characterized by age peaks at ca. 1.0 Ga, 1.4 Ga, and 1.6–1.7 Ga and intermediate to juvenile $\epsilon\text{Hf}(t)$ values of $+1.44$ to $+13.92$ and (2) youngest zircons between ca. 80 Ma and ca. 70 Ma that yield a more isotopically evolved $\epsilon\text{Hf}(t)$ range of -10.75 to -3.22 .

Crustal Evolution of Late Cretaceous Magmatism

Inherited ages recorded by zircon cores produced major age modes indicating sources from multiple crustal provinces: Grenville (1.1 Ga), Mazatzal (1.6–1.7 Ga), and Yavapai (1.7–1.8 Ga). Zircons derived from these Proterozoic crustal provinces typically result in intermediate to juvenile zircon $\epsilon\text{Hf}(t)$ values ranging from $+3$ to $+10$ (Fig. 9; Gehrels and Pecha, 2014; Mako et al., 2015; Chapman et al., 2018). $\epsilon\text{Hf}(t)$ ranges

of 1.1 Ga and 1.6–1.7 Ga ages, $+1$ to $+14$, are interpreted to have been derived from the Mazatzal and Yavapai provinces and are consistent with previous studies.

Middle Proterozoic inherited ages (1.4 Ga) consist of juvenile $\epsilon\text{Hf}(t)$ values, $+2.5$ to $+8.5$, similar to middle Proterozoic granitic rocks that are regionally observed in southeastern Arizona. During the middle Proterozoic (1.35–1.44 Ga), an extensive thermal episode related to intracontinental tectonism and plutonism was prominent in the southwestern U.S. and southern Rocky Mountains (Shaw and Karlstrom, 1999; Magrini et al., 2004; Shaw et al., 2005; Mako et al., 2015). This resulted in widespread emplacement of plutons such as the Oracle Pluton in the Santa Catalina Mountains ca. 50 km north of the Santa Rita Mountains. The Oracle Pluton was emplaced at 1.44 Ga in the Santa Catalina Mountains and is commonly associated with 1.6–1.7 Ga inherited core ages and juvenile $\epsilon\text{Hf}(t)$ values ranging from $+4$ to $+7.5$, similar to those in this study. The Oracle Pluton is extensive, 50 km across, and is interpreted to have deep-seated magmatic sources equivalent to those that provided abundant middle Proterozoic plutonic rocks (Fornash et al., 2013). Inherited zircon cores in this study are interpreted to have been derived from deep sources equivalent to the Oracle Pluton and others associated with the 1.35–1.44 Ga period of intracontinental tectonism.

Drewes (1971b) reported a K-Ar age of ca. 72 Ma for the Salero Formation, and Hayes (1986) estimated the intrusion cutting through the brown conglomerate to be Cenozoic in age based on stratigraphic relationships. Crystallization ages of the Salero Formation and the intrusion samples reported in this study are Late Cretaceous (ca. 75 Ma and 73 Ma) and postdate new maximum depositional ages from this study for the Fort Crittenden Formation of ca. 76 Ma. Lu-Hf isotopic values for Late Cretaceous zircon rims are evolved, -10.7 to -3.2 , and are consistent with previously reported $\epsilon\text{Hf}(t)$ values for Upper Cretaceous igneous rocks in the southwestern U.S. Cordillera of -7.5 to -15 (Fornash et al., 2013; Chapman et al., 2018). Under a compressional stress regime, magmas are often contaminated with old, thickened crust via melt extraction as subduction progresses and results in epsilon units following a distinct negative trend (Vervoort and Patchett, 1996). $\epsilon\text{Hf}(t)$ values for both old and young components of zircons from the samples studied fall along an average crustal evolution trend that indicates incorporation of older crustal provinces, including Yavapai-Mazatzal and middle Proterozoic plutonic rocks, from ca. 80–70 Ma.

THERMOCHRONOLOGY

Methods

We selected six samples from the Santa Rita Mountains for apatite fission track (AFT) and apatite (U-Th)/He (AHe) thermochronology (Figs. 2A and 3A). These samples include two granitic cobbles from the lower red conglomerate member, two Upper Cretaceous intrusion samples, and two Triassic volcanic samples from the Mount Wrightson Formation. The Mount Wrightson Formation and Upper Cretaceous intrusion samples were collected along a vertical transect along Mount Wrightson from roughly 2300 m to 2700 m. Samples from the Fort Crittenden Formation were limited in that granitic clasts large enough to yield enough apatite grains for fission track were only found in the first ~350 m of the lower red conglomerate member. Thermochronological sample locations from this study are reported in Table 2.

The AFT and AHe thermochronological techniques, when applied together, constrain the timing of cooling through the ~120 °C and ~45 °C temperature window (Reiners and Brandon, 2006, and references therein). Confined track length distributions in apatite provide information about the thermal history of a sample as it moves through the Partial Annealing Zone between ~120 °C and 60 °C (Gleadow et al., 1986).

Sample separates of apatite grains were prepared for AFT thermochronology and analyzed with the external detector method (Donelick et al., 1999; Donelick, 2005). Samples were mounted in epoxy and irradiated at Oregon State University and then mounted on glass slides for optical identification of fission tracks using an Olympus petrographic microscope at 1600 times magnification at the University of Arizona Fission Track Laboratory. The apatite grains were etched in 5.5 M nitric acid for 20 s at 21 °C according to methods outlined by Donelick et al. (1999), and mica prints were etched in 49% hydrofluoric acid for 15 min at 23 °C following Donelick (2005). For each sample, 20 grains were analyzed using the external detector method (Hurford and Green, 1983). All raw counting data are reported in the supplemental data files following the procedure of Flowers et al. (2015). Confined track lengths and diameters of fission track etch pits (Dpar) were measured in one of the granitic cobble clasts from the Fort Crittenden Formation (FC-AC17-7) and are reported in Table S5 (see footnote 1). Roughly 60 track lengths in total and two to six Dpar measurements per age determined grain were acquired from this sample to determine annealing kinetics and chemical composition (Donelick et al., 1999) and to then be utilized in thermo-kinetic modeling (Gallagher, 2012).

For AHe dating, single apatite crystals with a grain size >60 μm and without inclusions were photographed and measured for α-ejection corrections and then loaded into a niobium tube for analysis. The grains were then degassed by laser-heating using Nd:YAG and CO₂ lasers, and after cryogenic purification, the ⁴He was measured by quadrupole mass spectrometry (House et al., 2000). The degassed crystals were then dissolved in nitric acid, and the concentrations of U, Th, and Sm were measured using an ICP-MS. The α-ejection correction was then applied to the calculated AHe age to account for the loss of He that occurs within 20 μm of the crystal edge during the decay process (Farley, 1996; Ehlers and Farley, 2002). Estimated 2 sigma uncertainty is 6% for apatite He ages (Reiners et al., 2004).

Thermochronology modeling software QTQt (v. 5.7.0), developed by Gallagher (2012), was used to generate inverse thermal models that incorporate low-temperature thermochronologic data collected from sample FC-AC17-7 in the lower red conglomerate of the Fort Crittenden Formation in the Santa Rita Mountains. QTQt uses the Bayesian transdimensional Markov chain Monte Carlo inversion scheme with time-temperature points to construct a continuous thermal history through linear interpolation among sampled points (Gallagher, 2012). AFT ages, confined track length, Dpar, and AHe ages from sample FC-AC17-7 were modeled using QTQt. Model parameters are summarized in Table S6 (see footnote 1).

Thermochronological Results

All thermochronological ages are summarized in Table 3 and presented on radial plots and tables in the supplemental information (Fig. S2; Tables S3 and S4; see footnote 1). The following results are presented in two groups based on differences in lithology, elevation, and thermochronologic age in the following order: the Mount Wrightson transect samples and granitic cobbles from the lower red conglomerate member of the Fort Crittenden Formation (Fig. 3A).

Two lithologies were sampled in the Mount Wrightson transect and include Triassic volca-

nic rocks from the Mount Wrightson Formation and Upper Cretaceous intrusions that include the Josephine Canyon Diorite and the Madera Canyon Granodiorite. Volcanic rocks from the Mount Wrightson Formation were collected at the top of the transect at elevations of ca. 2700 m and 2300 m and did not provide AFT or AHe ages. The Josephine Canyon Diorite sample (MW18-3) was collected at ca. 2100 m and produced an AFT central age of 41.9 ± 5.7 Ma. The Madera Canyon Granodiorite sample (MW18-4) was collected at the base of the transect, at 1800 m, and produced an AFT central age of 44.94 ± 6.7 Ma. No AHe ages are available for samples along the Mount Wrightson transect.

The granitic samples from the Fort Crittenden Formation were collected at ca. 1500 m in elevation and at 50 m and 350 m within the lower red conglomerate member measured section (Fig. 3A). These samples (FC-AC17-7 and FC-AC18-2B) yielded AFT central ages of 26.86 ± 3.9 Ma and 34.1 ± 4.3 Ma, respectively. AHe ages, apatite confined fission track lengths, and Dpar data were collected for the latter (FC-AC17-7). Six AHe ages are between ca. 23 Ma and ca. 29 Ma (Table S4). Apatite confined fission track lengths show a bimodal distribution and mean track length of 11.5 μm (Fig. S3; see footnote 1). It should be noted that 100 measured track lengths are ideal for interpretation and thermal modeling, but due to the availability of measurable confined track lengths, only 60 were collected for this sample.

Thermal Modeling Results

Results from inverse modeling using QTQt are presented in this section for AFT and AHe data collected from one granitic cobble (FC-AC17-7) in the Fort Crittenden Formation in the Santa Rita Mountains. The QTQt inverse model results presented in this study were generated based on time-temperature paths for >100,000 model runs. The bimodal distribution observed in the confined track length indicates a complex two-phase cooling history during the Cenozoic that is observed in the inverse model. Results from this model indicate that the base of the Fort

TABLE 3. SUMMARY OF NEW THERMOCHRONOLOGIC AGES

Sample/type	Formation name (Ma)	AFT age (Ma ±1σ)	AHe age	
			(Ma)	Standard deviation (Ma)
FC-AC17-7 granitic clast	Fort Crittenden Formation	34.10 ± 4.35	25.43	0.27
			28.85	0.31
			23.31	0.25
			24.19	0.26
			23.16	0.25
			25.64	0.28
FC-AC18-2B granitic clast	Fort Crittenden Formation	26.86 ± 3.92	NA	NA
MW18-3 basement	Josephine Canyon Diorite	41.92 ± 5.74	NA	NA
MW18-4 basement	Madera Canyon Granodiorite	44.94 ± 6.72	NA	NA

Note: AFT—apatite fission track; AHe—apatite (U-Th)/He; NA—not applicable.

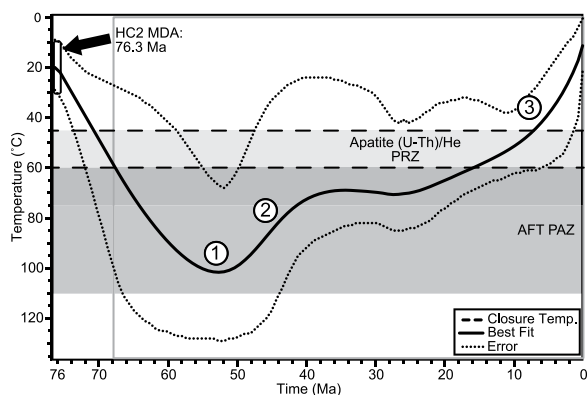


Figure 10. Best fit time–temperature paths from inverse modeling using QTQt are shown. This inverse model is based on apatite (U–Th)/He (AHe) ages and apatite fission track (AFT) age, length, and diameters of fission track etch pits (Dpar) measurements of a granitic cobble (FC-AC17-7) sampled in the lower red conglomerate member of the Fort Crittenden Formation in the Santa Rita Mountains. The

box outlined in black (top left) indicates the start time used in this model, which is the detrital zircon maximum depositional age at the top of the Fort Crittenden Formation (ca. 76 Ma). Dotted black lines show the envelope of good fit for the given parameters, and the thick solid black line shows the best fit time–temperature path. The dark gray shaded box indicates the AFT partial annealing zone (PAZ), and the light gray indicates the apatite (U–Th)/He partial retention zone (PRZ). AFT and AHe data tables and histograms are provided in the appendix. The number labels indicate (1) initial resetting at ca. 60–50 Ma followed by (2) the first phase of cooling at ca. 45–35 Ma and (3) the second phase cooling ca. 30–23 Ma.

Crittenden Formation was subjected to temperatures high enough to, at least partially, reset the AFT system during the Paleocene to Eocene (ca. 60–50 Ma) (Fig. 10). Following this heating, a first cooling episode (ca. 90–20 °C) is recorded between ca. 45 Ma and 35 Ma and a second cooling episode (ca. 90–40 °C) is recorded between ca. 30 Ma and 23 Ma (Fig. 10).

Interpretation

AFT and AHe ages, with thermal modeling, indicate Paleocene–Eocene post-depositional heating (resetting) followed by two periods of cooling during the middle Eocene and Oligocene (Fig. 10; Table 3). AFT ages from the Fort Crittenden Formation are interpreted to record resetting via post-depositional thermal overprinting during the middle Paleocene–early Eocene at ca. 60–50 Ma. The thickness of strata in the Fort Crittenden Formation and overlying units is estimated to be ~2 km, which is not enough to fully reset AFT and zircon fission track (ZFT) ages (Drewes, 1971b; Scarborough, 1989; Riley, 2004). Instead, Riley (2004) suggests that young reset detrital ZFT ages (ca. 55–44 Ma) in the Fort Crittenden Formation are the result of heating via an elevated regional geothermal gradient (30–35 °C/km) associated with Paleocene–early Eocene magmatism and subsequent relaxation of this elevated gradient in the Santa Rita Mountains. An elevated geothermal gradient between ca. 60 Ma and 50 Ma is consistent with the timing of emplacement of volcanic rocks in the Santa Rita Mountains (e.g., the Gringo Gulch

volcanic rocks; Fig. 2) and could explain initial resetting at the base of the Fort Crittenden Formation (Drewes, 1972a).

By ca. 45 Ma, magmatism in southeastern Arizona was extinguished as the arc migrated farther eastward into New Mexico (Dickinson, 1989; Humphreys, 1995; Constenius et al., 2003). The first phase of cooling at ca. 45–35 Ma is supported by both the inverse thermal model from the Fort Crittenden Formation cobble and by AFT data from Upper Cretaceous intrusions collected along the Mount Wrightson section in the Santa Rita Mountains (Fig. 10; Table 3). Cooling ages recorded by these samples predate the transition from crustal shortening to extension in the southwestern U.S. and are interpreted to preserve cooling via relaxation of the regional geothermal gradient (Constenius et al., 2003). The onset of crustal extension is marked by a westward sweep of magmatism at ca. 35 Ma and is generally attributed to westward rollback and subsequent foundering of the subducting Farallon slab (Coney and Reynolds, 1977; Constenius et al., 2003; Chapman et al., 2018).

AFT ages and inverse modeling results of samples in the Fort Crittenden Formation indicate a second phase of cooling during the Oligocene (starting at ca. 30 Ma) (Fig. 10; Table 3). Oligocene cooling can either be attributed to: (1) post-magmatic cooling following the westward sweep of magmatism or (2) extension related to metamorphic core complexes in southeastern Arizona. Although Oligocene igneous rocks are present in the Santa Rita Mountains, including

in the Gardener Canyon and Box Canyon dike swarms, and in the Grosvenor Hills volcanic rocks, the ages of these postdate the onset of Oligocene cooling by at least 3 m.y. Alternatively, this second phase of cooling was the result of footwall uplift and subsequent erosion via range-bounding normal faults mapped along the eastern flank of the Santa Rita Mountains by Drewes (1972b, 1996). This explanation is more consistent with the timing of regional normal faulting associated with metamorphic core complex extension (Coney and Reynolds, 1977; Constenius et al., 2003).

SUMMARY AND DISCUSSION

Sedimentary Basin Evolution

The conglomeratic facies of the lower red and brown conglomerate members of the Fort Crittenden Formation in the Santa Rita Mountains indicate deposition in a northeastward-flowing braided fluvial system supplied by local uplifts of Jurassic igneous rocks, the Bolsa Quartzite, and Paleozoic sedimentary rocks (Fig. 11B). A marked shift in paleodrainage is recorded with deposition of the upper red conglomerate, which indicates southwestward-flowing, sheet-flood-dominated alluvial fan deposition locally supplied by the uppermost Bisbee Group member, the Cintura Formation, to the northeast (Fig. 11C). Detrital zircon ages preserve overall trends of increasing co-magmatic grains (ca. 76 Ma) and decreasing Jurassic grains ca. (174–164 Ma; Fig. 7A). The up-section increase in both recycled sedimentary clasts and Proterozoic grains reflects a primary sediment source from the Cintura Formation. These depositional age zircons constrain a maximum depositional age of ca. 76 Ma for the top of the Fort Crittenden Formation consistent with ages of overlying volcanic rocks in the Salero Formation. The Fort Crittenden Formation in the Huachuca Mountains records deposition by braided streams and stream-dominated alluvial fans that drain south to southwestward (Fig. 11A; Hayes, 1986; and this study). Marginal lacustrine deposits begin at ~500 m in the Huachuca Mountains and record fluvial progradation into freshwater lacustrine environments (Figs. 6D and 11B). We interpret the abrupt change in depositional environments from the conglomerate member to the upper shale member, to be a result of extensive erosion that caused slope retreat along the mountain front, possibly located north to northeast of the Huachuca Mountains, and subsequent filling of the sedimentary basin (Fig. 11B). Conglomerate petrology and detrital zircon age spectra in the conglomerate member indicate a mixed

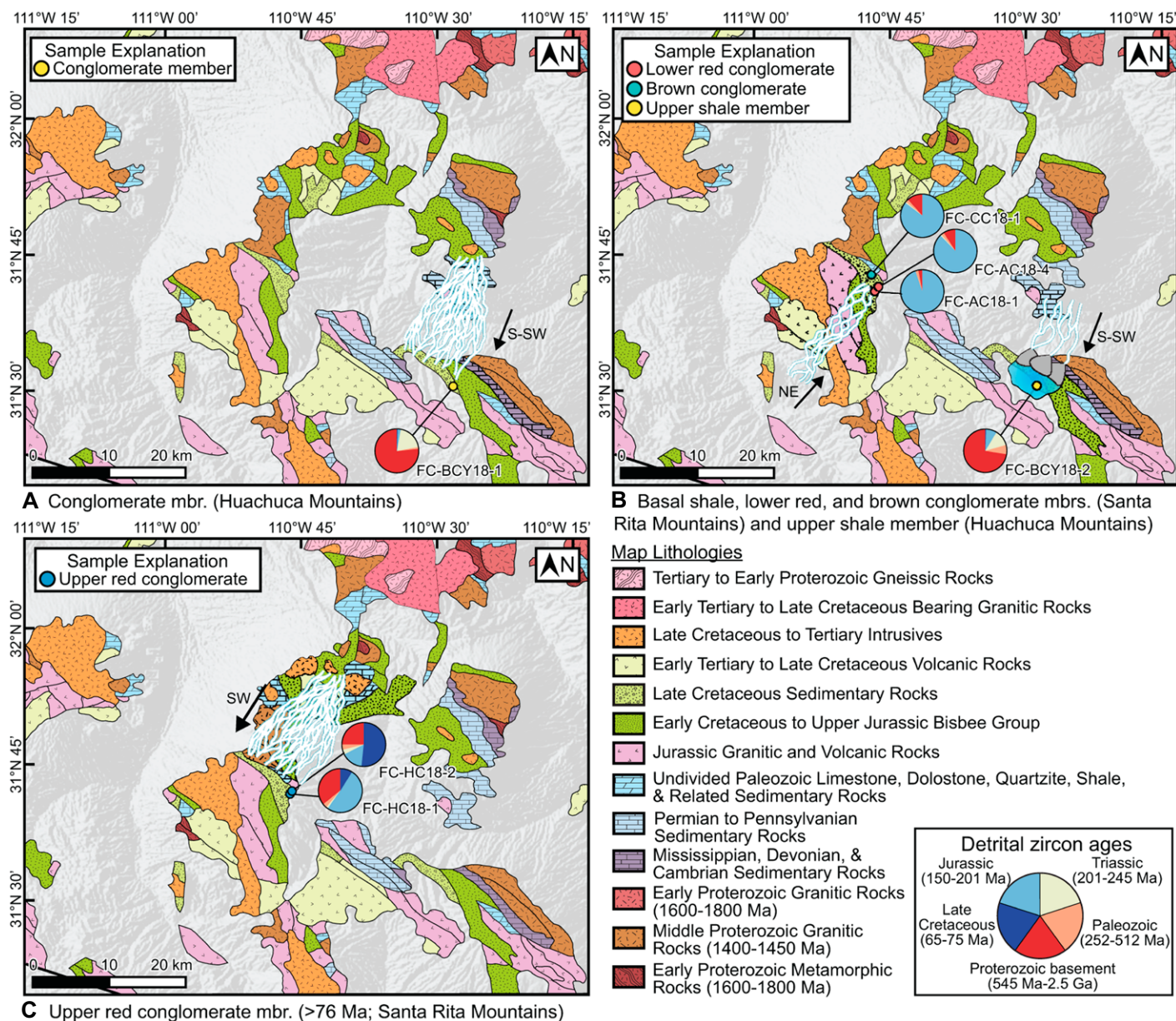


Figure 11. Paleogeographic reconstruction shows Late Cretaceous sediment transport in local depositional centers in the Huachuca Mountains (A–B) and the Santa Rita Mountains (B–C) resulting in deposition of the Fort Crittenden Formation. The geologic map depicts the detrital zircon signature of source lithologies in both depocenters. The paleodrainage system is depicted with white lines; the flow direction is depicted with a black arrow indicating direction. Detrital zircon ages for each sample are shown with pie charts. Provenance results, sedimentological analysis, and paleontological evidence suggest deposition between ca. 86 Ma and ca. 76 Ma in the Santa Rita Mountains (based on paleontological evidence and syndepositional zircons dated at 76 Ma) and that local depocenters experienced paleodrainage reorganization in response to active tectonics.

sediment source derived locally from Canelo Hills volcanic rocks, Proterozoic continental granodiorite, and Paleozoic sedimentary rocks (Figs. 6D and 7B). Detrital zircon U-Pb ages from the base of the conglomerate member and the top of the upper shale member represent slightly different sediment sources as indicated by MDS results (Fig. 8). This supports the

change in depositional environments recorded by the conglomerate and upper shale members.

Correlation of the Fort Crittenden Formation between the Santa Rita and Huachuca Mountains is difficult based on the sedimentary record alone as the Santa Rita Mountains record a change from fluvial to distal alluvial fan and the Huachuca Mountains record a change from

middle fan to distal fan to lacustrine environments. The earliest records of Late Cretaceous Laramide magmatism in southeastern Arizona aid in constraining maximum depositional ages and correlation between the Santa Rita and Huachuca Mountains. Based on MDA calculations and ages from paleontological evidence in the Santa Rita Mountains, we estimate deposition

between ca. 86 Ma and ca. 76 Ma. Based on the lack of depositional age zircons and stratigraphic relationships with the underlying Bisbee Group, we estimate that the Fort Crittenden Formation in the Huachuca Mountains was deposited after ca. 86 Ma but before ca. 76 Ma. The Cretaceous Seaway occupied the region until the Coniacian (ca. 90 Ma) (Merewether and McKinney, 2015). The fact that no marine deposits are present at the base of the Fort Crittenden Formation suggests that the base is younger than ca. 90 Ma. This is consistent with the estimated maximum depositional age at the base of the Fort Crittenden Formation, ca. 86 Ma, which is based on paleontological evidence. Sediment provenance information from conglomerate clast counts and detrital zircon analyses (2-D MDS) support our interpretation of sedimentation in isolated depocenters in the Santa Rita and Huachuca Mountains (Fig. 8). Additionally, the lack of depositional age zircons in the lower red and brown conglomerate members of the Santa Rita Mountains and throughout the entire formation in the Huachuca Mountains, suggests magmatic quiescence in southeastern Arizona prior to the eastward migration of arc magmatism into southeastern Arizona at ca. 76 Ma. Differences in sedimentary facies, complex drainage patterns, and local sources suggest sedimentation in isolated depocenters (Fig. 11). Based on regional correlations and the style of local sedimentation, paleodrainage, and provenance signal from this study, we interpret the Fort Crittenden Formation to have been deposited in a broken foreland basin setting no later than ca. 76 Ma (Dickinson et al., 1988; Lawton, 2008; Strecker et al., 2012; Capaldi et al., 2017). This is consistent with data from New Mexico showing that the Ringbone Basin records Laramide syntectonic deposition of a 2.4-km-thick group of fluvial to alluvial fan sedimentary rocks between ca. 75 Ma and 70 Ma (Clinkscales and Lawton, 2015) and suggests a possible eastward younging of Laramide-related basin development.

Laramide Magmatism

In the Santa Rita Mountains, the Salero Formation on top of the upper red conglomerate member records a transition from calc-alkaline to felsic volcanic rocks that are typical of a caldera system deposited between ca. 76 Ma and 72 Ma (Fig. 9; Lipman and Sawyer, 1985). $\epsilon\text{Hf}(t)$ values of post-depositional igneous rocks reflect magmas that evolved from contamination of old juvenile crust, i.e., incorporation of Yavapai-Mazatzal and middle Proterozoic plutonic rocks in the crustal melt (Fig. 9). Small volume and short-lived magmatism in Arizona at this time has been interpreted to represent

petit-spot melting driven by high stress bending related to the subducting slab (Axen et al., 2018).

Simultaneously, ca. 77–68 Ma, sediment that was deposited in the trench was subducted and then underplated across the southwestern U.S. Cordillera beginning at ca. 73 Ma and resulted in the Pelona-Orocopia-Rand (POR) schist (Grove et al., 2003; Jacobson et al., 2007; Seymour et al., 2018). The POR schist extends as far inboard as southeastern California and west-central Arizona and is suggested to be linked to magmatic arc extinction in the Mojave region (Fig. 1; Barth et al., 2008; Seymour et al., 2018). Emplacement of the POR schist and magmatic arc extinction in this region is interpreted as a direct result of flat slab subduction (Saleeby, 2003).

Cenozoic Thermal History

Our thermochronological data and thermal modeling results indicate Paleocene heating followed by a complex two-phase cooling history during middle Eocene and Oligocene time in the Santa Rita Mountains (Fig. 10). Initial resetting at ca. 60–50 Ma is recorded in samples at the base of the Fort Crittenden Formation and occurred due to an elevated geothermal gradient associated with Paleocene–early Eocene magmatism in southeastern Arizona. By ca. 45 Ma, magmatism in southeastern Arizona was extinguished and caused the regional geothermal gradient to relax (Dickinson, 1989; Humphreys, 1995; Constenius et al., 2003). The first phase of cooling at ca. 45–35 Ma is interpreted to reflect cooling via relaxation of the geothermal gradient (Fig. 10). During late Eocene time (ca. 35 Ma), the tectonic regime in southeastern Arizona transitioned from crustal shortening to extension and resulted in normal faulting and metamorphic core complex extension. The timing of the second phase of cooling between ca. 30 Ma and 23 Ma is consistent with regional normal faulting and can be explained by possible tectonic exhumation via range-bounding normal faults (Fig. 10).

CONCLUSIONS

Our results indicate that the Fort Crittenden Formation in southeastern Arizona was deposited in local depocenters between ca. 86 Ma and ca. 76 Ma. The style of sedimentation and complex drainage pattern is consistent with a broken foreland basin setting related to Laramide style tectonics. Uplift of local ranges due to Laramide deformation was followed by a pulse of magmatism in the Santa Rita Mountains starting at ca. 76 Ma with the Salero Formation and ending at ca. 50 Ma. Evolved $\epsilon\text{Hf}(t)$ values of Late Cretaceous igneous rocks indicate contamination of melt with older crustal material due to the inland

migration of magmatism. Our data indicate that simultaneous Laramide magmatism in southeastern Arizona and flat slab-related emplacement of the POR schist north of our field area suggest a complex slab geometry in the southwestern U.S. Cordillera during the Late Cretaceous that is consistent with the southern extent of the flat slab in west-central Arizona (Bird, 1984). Additionally, our age results support the southwestern to northeastern migration of the Laramide deformation and magmatic front from southeast Arizona, to south-central New Mexico indicated by syntectonic units in the Ringbone Basin at ca. 75–70 Ma and the Love Ranch Basin in the early Paleogene (Clinkscales and Lawton, 2015; McMillan, 2004). We interpret this migration to have been driven by progressive shallowing of the subducted Farallon slab (Coney and Reynolds, 1977; Keith, 1978; Dickinson, 1989; Clinkscales and Lawton, 2018).

Magmatic activity persisted in the Santa Rita Mountains until ca. 50 Ma. Our new AFT data, AHe data, and thermal models indicate Paleogene heating associated with magmatism, Eocene (ca. 50–40 Ma) cooling, and a second phase of cooling starting at ca. 30 Ma. The transition from crustal shortening to extension by ca. 35 Ma can explain the second phase of cooling during the Oligocene. Cooling between ca. 30 Ma and 23 Ma records possible tectonic exhumation via normal faulting and metamorphic core complex extension. Our data constrain models for development of the southwestern U.S. Cordillera and show that intermontane, Laramide-style basin deposition occurred in southern Arizona between ca. 86 Ma and ca. 76 Ma, and was followed by small scale Upper Cretaceous magmatism and subsequent Cenozoic cooling and exhumation.

ACKNOWLEDGMENTS

This research was funded by National Science Foundation (NSF) grants EAR-1524151 and EAR-1649254 for support of the Arizona LaserChron Center. We thank the *GSA Bulletin* Associate Editor and two anonymous reviewers for guidance on how to improve this manuscript. We gratefully acknowledge guidance from George Gehrels for useful scientific discussions and feedback on early versions of this manuscript. We thank staff at the Arizona LaserChron Center for assistance in acquiring and discussing the U-Pb data. New detrital zircon U-Pb geochronologic data are reported in the supplemental data files and are archived at geochron.org. Gilby Jepson provided guidance in thermal modeling. We thank Shlomo Honig for feedback on the figures.

REFERENCES CITED

- Allen, P.A., Institut, G., and Bern, U., 1981, Sediments and processes on a Sm: *Sedimentary Geology*, v. 29, p. 31–66.
 Asmerom, Y., Zartman, R.E., Damon, P.E., and Shafiqullah, M., 1990, Zircon U-Th-Pb and whole-rock Rb-Sr

- age patterns of lower Mesozoic igneous rocks in the Santa Rita Mountains, southeast Arizona: Implications for Mesozoic magmatism and tectonics in the southern Cordillera: *Geological Society of America Bulletin*, v. 102, p. 961–968, [https://doi.org/10.1130/0016-7606\(1990\)102<0961:ZUTPAW>2.3.CO;2](https://doi.org/10.1130/0016-7606(1990)102<0961:ZUTPAW>2.3.CO;2).
- Axen, G.J., van Wijk, J.W., and Currie, C.A., 2018, Basal continental mantle lithosphere displaced by flat-slab subduction: *Nature Geoscience*, v. 11, p. 961–964, <https://doi.org/10.1038/s41561-018-0263-9>.
- Barth, A.P., Wooden, J.L., Jacobson, C.E., and Probst, K., 2004, U-Pb geochronology and geochemistry of the McCoy Mountains Formation, southeastern California: A Cretaceous retroarc foreland basin: *Geological Society of America Bulletin*, v. 116, p. 142–153, <https://doi.org/10.1130/B25288.1>.
- Barth, A.P., Wooden, J.L., Howard, K.A., and Richards, J.L., 2008, Late Jurassic plutonism in the southwest U.S. Cordillera, in Wright, J.E., and Shervais, J.W., eds., *Ophiolites, Arcs and Batholiths: A Tribute to Cliff Hopson: Geological Society of America Special Paper 438*, p. 379–396, [https://doi.org/10.1130/B25288.110.1130/2008.2438\(13\)](https://doi.org/10.1130/B25288.110.1130/2008.2438(13)).
- Bassett, K.N., and Busby, C.J., 2005, Tectonic setting of the glance conglomerate along the sawmill canyon fault zone, southern Arizona: A sequence analysis of an intra-arc strike-slip basin, in Anderson, T.H., Nourse, J.A., McKee, J.W., and Steiner, M.B., eds., *The Mojave-Sonora Megasear Hypothesis: Development, Assessment, and Alternatives: Geological Society of America Special Paper 393*, p. 377–400, <https://doi.org/10.1130/0-8137-2393-0.377>.
- Bird, P., 1984, Laramide crustal thickening event in the Rocky Mountain Foreland and Great Plains: *Tectonics*, v. 3, p. 741–758.
- Bird, P., 1998, Kinematic history of the Laramide orogeny in latitudes 35°–49°N, western United States: *Tectonics*, v. 17, p. 780–801.
- Black, L.P., et al., 2004, Improved ²⁰⁶Pb/²³⁸U microprobe geochronology by the monitoring of a trace-element-related matrix effect; SHRIMP, ID-TIMS, ELA-ICP-MS and oxygen isotope documentation for a series of zircon standards: *Chemical Geology*, v. 205, p. 115–140, <https://doi.org/10.1016/j.chemgeo.2004.01.003>.
- Bluck, B.J., 1964, Sedimentation of an alluvial fan in southern Nevada: *SEPM Journal of Sedimentary Research*, v. 34, <https://doi.org/10.1306/74d71078-2b21-11d7-8648000102c1865d>.
- Busby-Spera, C.J., Martinson, J.M., Riggs, N.R., and Schermer, E.R., 1990, The Triassic-Jurassic magmatic arc in the Mojave-Sonoran deserts and the Sierran-Klamath region: Similarities and differences in paleogeographic evolution, in Harwood, D.S., and Miller, M.M., eds., *Paleozoic and Early Mesozoic Paleogeographic Relations: Sierra Nevada, Klamath Mountains, and Related Terranes: Geological Society of America Special Paper 255*, p. 325–337, <https://doi.org/10.1130/SPE255-p325>.
- Cant, D.J., and Walker, R.G., 1978, Fluvial processes and facies sequences in the sandy braided South Saskatchewan River, Canada: *Sedimentology*, v. 25, p. 625–648, <https://doi.org/10.1111/j.1365-3091.1978.tb00323.x>.
- Capaldi, T.N., Horton, B.K., McKenzie, N.R., Stockli, D.F., and Odlum, M.L., 2017, Sediment provenance in contractional orogens: The detrital zircon record from modern rivers in the Andean fold-thrust belt and foreland basin of western Argentina: *Earth and Planetary Science Letters*, v. 479, p. 83–97, <https://doi.org/10.1016/j.epsl.2017.09.001>.
- Cecil, M.R., Gehrels, G.E., Ducea, M.N., and Patchett, P.J., 2011, U-Pb-Hf characterization of the central Coast Mountains batholith: Implications for petrogenesis and crustal architecture: *Lithosphere*, v. 3, p. 247–260, <https://doi.org/10.1130/L134.1>.
- Chapin, C.E., and Cather, S.M., 1983, Eocene tectonics and sedimentation in the Colorado Plateau-Rocky Mountain area: *Rocky Mountain Foreland Basins and Uplifts*, p. 33–56.
- Chapman, A.D., 2017, The Pelona–Orocopia–Rand and related schists of southern California: A review of the best-known archive of shallow subduction on the planet: *International Geology Review*, v. 59, p. 664–701, <https://doi.org/10.1080/00206814.2016.1230836>.
- Chapman, J.B., Dufov, M.N., Gehrels, G.E., Ducea, M.N., Valley, J.W., and Ishida, A., 2018, Lithospheric architecture and tectonic evolution of the southwestern U.S. Cordillera: Constraints from zircon Hf and O isotopic data: *Geological Society of America Bulletin*, v. 130, p. 2031–2046, <https://doi.org/10.1130/B31937.1>.
- Clinkscales, C.A., and Lawton, T.F., 2015, Timing of Late Cretaceous shortening and basin development, Little Hatched Mountains, southwestern New Mexico, USA—Implications for regional Laramide tectonics: *Basin Research*, v. 27, p. 453–472, <https://doi.org/10.1111/bre.12083>.
- Clinkscales, C.A., and Lawton, T.F., 2018, Mesozoic–Paleogene structural evolution of the southern U.S. Cordillera as revealed in the Little and Big Hatched Mountains, southwest New Mexico, USA: *Geosphere*, v. 14, p. 162–186, <https://doi.org/10.1130/GES01539.1>.
- Coney, P.J., 1972, Cordilleran tectonics and North America plate motion: *American Journal of Science*, v. 272, p. 603–628, <https://doi.org/10.2475/ajs.272.7.603>.
- Coney, P.J., and Reynolds, S.J., 1977, Cordilleran Benioff Zones: *Nature*, v. 270, p. 403–406, <https://doi.org/10.1038/270403a0>.
- Constenius, K., 1996, Late Paleogene extensional collapse of the Cordilleran foreland fold and thrust belt: *Geological Society of America Bulletin*, v. 108, p. 20–39, [https://doi.org/10.1130/0016-7606\(1996\)108<0020:LPECO T>2.3.CO;2](https://doi.org/10.1130/0016-7606(1996)108<0020:LPECO T>2.3.CO;2).
- Constenius, K., Esser, R.P., and Layer, P.W., 2003, Extensional collapse of the Charleston-Nebo Salient and its relationship to space-time variations in Cordilleran orogenic belt tectonism and continental stratigraphy, in Reynolds, R.G., and Flores, R.M., eds., *Cenozoic Systems of the Rocky Mountain Region: Denver, Colorado, SEPM (Society for Sedimentary Geology) Rocky Mountain Section*, p. 303–343.
- Copeland, P., Currie, C.A., Lawton, T.F., and Murphy, M.A., 2017, Location, location, location: The variable lifespan of the Laramide orogeny: *Geology*, v. 45, p. 223–226, <https://doi.org/10.1130/G38810.1>.
- Cross, T.A., and Pilger, R.H., 1978, Tectonic controls of Late Cretaceous sedimentation, western interior, USA: *Nature*, v. 274, p. 653–657, <https://doi.org/10.1038/274653a0>.
- Dalman, S.G., Hodnett, J.-P.M., Lichtig, A.J., and Lucas, S.G., 2018, A new ceratopsid dinosaur (Centrosaurinae: Nasutoceratopsina) from the Fort Crittenden Formation, Upper Cretaceous (Campanian) of Arizona: *New Mexico Museum of Natural History and Science Bulletin*, v. 79, p. 141–164.
- Davis, G.H., 1979, Laramide folding and faulting in Southeastern Arizona: *American Journal of Science*, v. 279, p. 543–569, <https://doi.org/10.2475/ajs.279.5.543>.
- DeCelles, P.G., 2004, Late Jurassic to Eocene evolution of the Cordilleran: *American Journal of Science*, v. 304, p. 105–168, <https://doi.org/10.2475/ajs.304.2.105>.
- DeCelles, P.G., Gray, M.B., Ridgway, K.D., Cole, R.B., Pivnik, D.A., Pequera, N., and Srivastava, P., 1991, Controls on synorogenic alluvial fan architecture, Beartooth Conglomerate (Palaeocene), Wyoming and Montana: *Sedimentology*, v. 38, p. 567–590, <https://doi.org/10.1111/j.1365-3091.1991.tb01009.x>.
- Dickinson, W.R., 1989, Tectonic setting of Arizona through geologic time: *Arizona Geological Society Digest*, v. 17, p. 1–16.
- Dickinson, W.R., 2003, Excursion to Gardner Canyon: Sedimentology and tectonic context of Mesozoic strata in the Santa Rita Mountains, southeastern Arizona: *Tucson, Arizona Geological Survey Contributed Report*, 29 p.
- Dickinson, W.R., 2004, Evolution of the North American Cordillera: *Annual Review of Earth and Planetary Sciences*, v. 32, p. 13–45, <https://doi.org/10.1146/annurev.earth.32.101802.120257>.
- Dickinson, W.R., and Gehrels, G.E., 2008, Sediment delivery to the Cordilleran foreland basin: Insights from U-Pb ages of detrital zircons in Upper Jurassic and Cretaceous strata of the Colorado Plateau: *American Journal of Science*, v. 308, p. 1041–1082, <https://doi.org/10.2475/10.2008.01>.
- Dickinson, W.R., and Gehrels, G.E., 2009, U-Pb ages of detrital zircons in Jurassic eolian and associated sandstones of the Colorado plateau: Evidence for transcontinental dispersal and intraregional recycling of sediment: *Geological Society of America Bulletin*, v. 121, p. 408–433, <https://doi.org/10.1130/B26406.1>.
- Dickinson, W.R., and Lawton, T.F., 2001, Carboniferous to Cretaceous assembly and fragmentation of Mexico: *Geological Society of America Bulletin*, v. 113, p. 1142–1160, [https://doi.org/10.1130/0016-7606\(2001\)113<1142:CTCAAF>2.0.CO;2](https://doi.org/10.1130/0016-7606(2001)113<1142:CTCAAF>2.0.CO;2).
- Dickinson, W.R., and Snyder, W.S., 1978, Plate tectonics of the Laramide orogeny, in Matthews III, V., ed., *Laramide Folding Associated with Basement Block Faulting in the Western United States: Geological Society of America Memoir 151*, p. 355–366, <https://doi.org/10.1130/MEM151-p355>.
- Dickinson, W.R., Klute, M.A., Hayes, M.J., Janecke, S.U., Lundin, E.R., McKittrick, M.A., and Olivares, M.D., 1988, Paleogeographic and paleotectonic setting of Laramide sedimentary basins in the central Rocky Mountain region: *Geological Society of America Bulletin*, v. 100, p. 1023–1039, [https://doi.org/10.1130/0016-7606\(1988\)100<1023:PAPSO L>2.3.CO;2](https://doi.org/10.1130/0016-7606(1988)100<1023:PAPSO L>2.3.CO;2).
- Dickinson, W.R., Fiorillo, A.R., Hall, D.L., Rogelio, M., and Potochnik, A.R., 1989, Cretaceous strata of southern Arizona: *Arizona Geological Society Digest*, v. 17, p. 447–461.
- Dickinson, W.R., Lawton, T.F., and Gehrels, G.E., 2009, Recycling detrital zircons: A case study from the Cretaceous Bisbee Group of southern Arizona: *Geology*, v. 37, p. 503–506, <https://doi.org/10.1130/G25646A.1>.
- Donelick, R.A., 2005, Apatite fission-track analysis: Reviews in Mineralogy and Geochemistry, v. 58, p. 49–94, <https://doi.org/10.2138/rmg.2005.58.3>.
- Donelick, R.A., Ketchum, R.A., and Carlson, W.D., 1999, Variability of apatite fission-track annealing kinetics: II. Crystallographic orientation effects: *The American Mineralogist*, v. 84, p. 1224–1234, <https://doi.org/10.2138/am-1999-0902>.
- Drewes, H.D., 1971a, Geologic map of the Mount Wrightson quadrangle, southeast of Tucson, Santa Cruz and Pima Counties, Arizona: *U.S. Geological Survey Miscellaneous Geologic Investigations Map I-614*, scale 1:48,000.
- Drewes, H.D., 1971b, Mesozoic Stratigraphy of the Santa Rita Mountains, Southeast of Tucson, Arizona: *U.S. Geological Survey Professional Paper 658-C*, 80 p.
- Drewes, H.D., 1972a, Cenozoic rocks of the Santa Rita Mountains, Southeast of Tucson, Arizona: *U.S. Geological Survey Professional Paper 746*, 66 p.
- Drewes, H.D., 1972b, Structural geology of the Santa Rita Mountains, southeast of Tucson, Arizona: *U.S. Geological Survey Professional Paper 748*, 35 p., <https://pubs.usgs.gov/pp/0748/report.pdf>.
- Drewes, H.D., 1976, Plutonic rocks of the Santa Rita Mountains, southeast of Tucson, Arizona: *U.S. Geological Survey Professional Paper 915*, 75 p., <https://doi.org/10.3133/pp915>.
- Drewes, H.D., 1978, The Cordilleran orogenic belt between Nevada and Chihuahua: *Geological Society of America Bulletin*, v. 89, p. 641–657, [https://doi.org/10.1130/0016-7606\(1978\)89<641:TCOBBN>2.0.CO;2](https://doi.org/10.1130/0016-7606(1978)89<641:TCOBBN>2.0.CO;2).
- Drewes, H.D., 1991, Description and development of the Cordilleran orogenic belt in the southwestern United States and northern Mexico: *U.S. Geological Survey Professional Paper 1512*, scales 1:50,000 and 1:24,000, 2 sheets, 92 p.
- Drewes, H.D., 1996, Geology of Coronado National Forest: *U.S. Geological Survey*, scale 1:126,720, plate 4, <https://doi.org/10.3133/b2083AK>.
- Ducea, M., 2001, The California arc: Thick granitic batholiths, eclogitic residues, lithospheric-scale thrusting, and magmatic flare-ups: *GSA Today*, v. 11, p. 4–10, [https://doi.org/10.1130/1052-5173\(2001\)011<0004:TCATGB>2.0.CO;2](https://doi.org/10.1130/1052-5173(2001)011<0004:TCATGB>2.0.CO;2).
- Ehlers, T., and Farley, K.A., 2002, Apatite (U-Th)/He thermochronometry: methods and applications to problems in tectonic and surface processes: *Earth and Planetary Science Letters*, v. 206, p. 1–14, [https://doi.org/10.1016/S0012-821X\(02\)01069-5](https://doi.org/10.1016/S0012-821X(02)01069-5).
- Engelbreton, D.C., Cox, A., and Thompson, G.A., 1984, Correlation of plate motions with continental tectonics: *Laramide to basin-range: Tectonics*, v. 3, p. 115–119.

- Erslev, E.A., 1993, Thrusts, backthrusts and detachment of Laramide foreland arches: Laramide basement deformation in the Rocky Mountain foreland of the western United States, *in* Schmidt, C.J., et al., eds., *Laramide Basement Deformation in the Rocky Mountain Foreland of the Western United States*: Geological Society of America Special Paper 280, p. 125–146, <https://doi.org/10.1130/SPE280-p125>.
- Farley, K.A., 2002, (U-Th)/He Dating: Techniques, Calibrations, and Applications: Reviews in Mineralogy and Geochemistry, v. 47, no. 1, p. 819–844, <https://doi.org/10.2138/rmg.2002.47.18>.
- Favorito, D.A., and Seedorf, E., 2017, Characterization and reconstruction of Laramide shortening and superimposed Cenozoic extension, Romero Wash-Tecolote Ranch area, southeastern Arizona: *Geosphere*, v. 13, p. 577–607, <https://doi.org/10.1130/GES01381.1>.
- Ferguson, C.A., Youberg, A., Gilbert, W.G., Orr, T.R., Richard, S.M., and Spencer, J.E., 2001, Geologic map of the Mount Fagan 7.5' quadrangle, eastern Pima County, Arizona: Arizona Geological Survey Digital Geologic Map, v. 11, scale 1:24,000, 1 sheet, 36 p.
- Flowers, R.M., Farley, K.A., and Ketcham, R.A., 2015, A reporting protocol for thermochronologic modeling illustrated with data from the Grand Canyon: *Earth and Planetary Science Letters*, v. 432, p. 425–435, <https://doi.org/10.1016/j.epsl.2015.09.053>.
- Fornash, K.F., Patchett, P.J., Gehrels, G.E., and Spencer, J.E., 2013, Evolution of granitoids in the Catalina metamorphic core complex, southeastern Arizona: U-Pb, Nd, and Hf isotopic constraints: Contributions to Mineralogy and Petrology, v. 165, p. 1295–1310, <https://doi.org/10.1007/s00410-013-0859-4>.
- Gallagher, K., 2012, Transdimensional inverse thermal history modeling for quantitative thermochronology: *Journal of Geophysical Research: Solid Earth*, v. 117, p. 1–16, <https://doi.org/10.1029/2011JB008825>.
- Gehrels, G.E., and Pecha, M., 2014, Detrital zircon U-Pb geochronology and Hf isotope geochemistry of Paleozoic and Triassic passive margin strata of western North America: *Geosphere*, v. 10, p. 49–65, <https://doi.org/10.1130/GES00889.1>.
- Gehrels, G.E., Valencia, V.A., and Ruiz, J., 2008, Enhanced precision, accuracy, efficiency, and spatial resolution of U-Pb ages by laser ablation-multicollector-inductively coupled plasma-mass spectrometry: *Geochemistry, Geophysics, Geosystems*, v. 9, p. 1–13, <https://doi.org/10.1029/2007GC001805>.
- Gleadow, A.J.W., Duddy, I.R., Green, P.F., and Lovering, J.F., 1986, Confined fission track lengths in apatite: A diagnostic tool for thermal history analysis: Contributions to Mineralogy and Petrology, v. 94, p. 405–415, <https://doi.org/10.1007/BF00376334>.
- Gross, E.L., Stewart, J.H., and Gehrels, G.E., 2000, Detrital zircon geochronology of Neoproterozoic to Middle Cambrian miogeoclinal and platformal strata: Northwest Sonora, Mexico: *Geofísica Internacional*, v. 39, p. 295–308, <https://doi.org/10.22201/igef.00167169p.2000.39.4.241>.
- Grove, M., Jacobson, C.E., Barth, A.P., and Vucic, A., 2003, Temporal and spatial trends of Late Cretaceous-early Tertiary underplating of Pelona and related schist beneath southern California and southwestern Arizona, *in* Johnson, S.E., Paterson, S.R., Fletcher, J.M., Girty, G.H., Kimbrough, D.L., and Martín-Barajas, A., eds., *Tectonic Evolution of Northwestern Mexico and the Southwestern USA*: Geological Society of America. Special Paper 374, p. 381–406, <https://doi.org/10.1130/0-8137-2374-4.381>.
- Hayes, M.J., 1986, Sedimentology, stratigraphy, and paleogeography of the Fort Crittenden Formation (Upper Cretaceous), southeastern Arizona [M.S. thesis]: Tucson, University of Arizona, 117 p., <http://azgs.arizona.edu/azgeobib/sedimentology-stratigraphy-and-paleogeography-fort-crittenden-formation-upper-cretaceous>.
- Hayes, P.T., 1970a, Cretaceous paleogeography of southeastern Arizona and adjacent areas: U.S. Geological Survey Professional Paper 658-B, 42 p., <https://doi.org/10.3133/pp658B>.
- Hayes, P.T., 1970b, Mesozoic stratigraphy of the Mule and Huachuca Mountains, Arizona: U.S. Geological Survey Professional Paper 658-A, 45 p., <https://doi.org/10.3133/pp658A>.
- Hayes, P.T., and Drewes, H.D., 1978, Mesozoic depositional history of southeastern Arizona, *in* Callender, J.F., Wilt, J.C., and Clemons, R.C., eds., *Land of Cochise, Southeastern Arizona*: New Mexico Geological Society in cooperation with the Arizona Geological Society, 29th Field Conference, p. 201–207.
- Hayes, P.T., and Raup, R.B., 1968, Geologic map of the Huachuca and Mustang Mountains, southeastern Arizona: U.S. Geological Survey, scale 1:48,000, 1 sheet, <https://doi.org/10.3133/i509>.
- Heckert, A.B., Lucas, S.G., and Krzyzanowski, S.E., 2003, Vertebrate fauna of the late Campanian (Judithian) Fort Crittenden Formation, and the age of Cretaceous vertebrate faunas of southeastern Arizona (USA): *Neues Jahrbuch für Geologie und Paläontologie. Abhandlungen*, v. 227, p. 343–364.
- Henderson, L.J., Gordon, R.G., and Engebretson, D.C., 1984, Mesozoic aseismic ridges on the Farallon plate and southward migration of shallow subduction during the Laramide orogeny: *Tectonics*, v. 3, p. 121–132, <https://doi.org/10.1029/TC0031002p00121>.
- Holk, G.J., Grove, M., Jacobson, C.E., and Haxel, G.B., 2017, A two-stage fluid history for the Orocopia Schist and associated rocks related to flat subduction and exhumation, southeastern California: *International Geology Review*, v. 59, p. 639–663, <https://doi.org/10.1080/00206814.2016.1227729>.
- Horstwood, M.S.A., Köslér, J., Gehrels, G., Jackson, S.E., McLean, N.M., Paton, C., Pearson, N.J., Sircombe, K., Sylvester, P., Vermeesch, P., Bowring, J.F., Condon, D.J., and Schoene, B., 2016, Community-derived standards for LA-ICP-MS U-(Th)-Pb Geochronology—Uncertainty propagation, age interpretation and data reporting: *Geostandards and Geoanalytical Research*, v. 40, p. 311–332, <https://doi.org/10.1111/j.1751-908X.2016.00379.x>.
- House, M.A., Farley, K.A., and Stockli, D., 2000, Helium chronometry of apatite and titanite using Nd-YAG laser heating: *Earth and Planetary Science Letters*, v. 183, p. 365–368, [https://doi.org/10.1016/S0012-821X\(00\)00286-7](https://doi.org/10.1016/S0012-821X(00)00286-7).
- Humphreys, E.D., 1995, Post-Laramide removal of the Farallon slab, western United States: *Geology*, v. 23, p. 987–990, [https://doi.org/10.1130/0091-7613\(1995\)023<0987:PLROTF>2.3.CO;2](https://doi.org/10.1130/0091-7613(1995)023<0987:PLROTF>2.3.CO;2).
- Humphreys, E.D., 2009, Relation of flat subduction to magmatism and deformation in the western United States, *in* Mahlburg Kay, S., Ramos, V.A., and Dickinson, W.R., eds., *Backbone of the Americas: Shallow Subduction, Plateau Uplift, and Ridge and Trench Collision*: Geological Society of America Memoir 204, p. 85–98, [https://doi.org/10.1130/2009.1204\(04\)](https://doi.org/10.1130/2009.1204(04)).
- Humphreys, E.D., Schmandt, B., Bezada, M.J., and Perry-Houts, J., 2015, Recent craton growth by slab stacking beneath Wyoming: *Earth and Planetary Science Letters*, v. 429, p. 170–180, <https://doi.org/10.1016/j.epsl.2015.07.066>.
- Hurfurd, A.J., and Green, P.F., 1983, The zeta age calibration of fission-track dating: *Chemical Geology*, v. 41, p. 285–317, [https://doi.org/10.1016/S0009-2541\(83\)80026-6](https://doi.org/10.1016/S0009-2541(83)80026-6).
- Ibanez-Mejia, M., Gehrels, G.E., Ruiz, J., Vervoort, J.D., Eddy, M.E., and Li, C., 2014, Small-volume baddeleyite (ZrO₂) U-Pb geochronology and Lu-Hf isotope geochemistry by LA-ICP-MS. Techniques and applications: *Chemical Geology*, v. 384, p. 149–167, <https://doi.org/10.1016/j.chemgeo.2014.07.011>.
- Inman, K.F., 1987, Depositional environments and sandstone petrography of Upper Cretaceous sedimentary rocks, Adobe Canyon, Santa Rita Mountains, southeast Arizona: Arizona Geological Society Digest, v. 18, p. 301–314.
- Jacobson, C.E., Grove, M., Vučić, A., Pedrick, J.N., and Ebert, K.A., 2007, Exhumation of the Orocopia Schist and associated rocks of southeastern California: Relative roles of erosion, synsubduction tectonic denudation, and middle Cenozoic extension, *in* Cloos, M., Carlson, W.D., Gilbert, M.C., Liou, J.G., and Sorensen, S.S., eds., *Convergent Margin Terranes and Associated Regions: A Tribute to W.G. Ernst*: Geological Society of America Special Paper 419, p. 1–37, [https://doi.org/10.1130/2007.2419\(01\)](https://doi.org/10.1130/2007.2419(01)).
- Jones, C.H., Farmer, G.L., Sageman, B., and Zhong, S., 2011, Hydrodynamic mechanism for the Laramide orogeny: *Geosphere*, v. 7, p. 183–201, <https://doi.org/10.1130/GES00575.1>.
- Jordan, T.E., 1981, Thrust loads and foreland basin evolution, Cretaceous, Western United States: *American Association of Petroleum Geologists Bulletin*, v. 65, p. 2506–2520.
- Jordan, T.E., and Allmendinger, R.W., 1986, The Sierras Pampeanas of Argentina; a modern analogue of Rocky Mountain foreland deformation: *American Journal of Science*, v. 286, p. 737–764, <https://doi.org/10.2475/ajs.286.10.737>.
- Keith, S.B., 1978, Paleosubduction geometries inferred from Cretaceous and Tertiary magmatic patterns in southwestern North America: *Geology*, v. 6, p. 516–521, [https://doi.org/10.1130/0091-7613\(1978\)6<516:PGIFCA>2.0.CO;2](https://doi.org/10.1130/0091-7613(1978)6<516:PGIFCA>2.0.CO;2).
- Keith, S.B., and Wilt, J.C., 1986, Laramide orogeny in Arizona and adjacent regions: A stratotectonic synthesis, *in* Beatty, B., and Wilkinson, P.A.K., eds., *Frontiers in Geology and Ore Deposits of Arizona and the Southwest*: Arizona Geological Society Digest, v. 16, p. 502–554.
- Krantz, R., 1989, Laramide structures of Arizona: *Geologic Evolution of Arizona*: Arizona Geological Society Digest, v. 17, p. 463–483.
- Krebs, C.K., and Ruiz, J., 1987, Geochemistry of the Canelo Hills volcanics and implications for the Jurassic tectonic setting of southeastern Arizona, *in* Dickinson, W.R., and Klute, M.A., eds., *Mesozoic Rocks of Southern Arizona and Adjacent Areas*: Arizona Geological Society Digest, v. 18, p. 139–151.
- Lawton, T.F., 2008, Chapter 12 Laramide Sedimentary Basins, *in* Lawton, T.F., ed., *Sedimentary Basins of the World*: Elsevier, v. 5, p. 429–450, [https://doi.org/10.1016/S1874-5997\(08\)00012-9](https://doi.org/10.1016/S1874-5997(08)00012-9).
- Lawton, T.F., Amato, J.M., Machin, S.E.K., Gilbert, J.C., and Lucas, S.G., 2020, Transition from Late Jurassic rifting to middle Cretaceous dynamic foreland, southwestern U.S. and northwestern Mexico: *Geological Society of America Bulletin*, v. 132, p. 2489–2516, <https://doi.org/10.1130/B35433.1>.
- Lindberg, F.A., 1987, Cretaceous Sedimentary Geology of the Rucker Canyon Area, Cochise County, Arizona, *in* Dickinson, W.R., and Klute, M.A., eds., *Mesozoic Rocks of Southern Arizona and Adjacent Areas*: Arizona Geological Society Digest, v. 18, p. 283–299.
- Lipman, P.W., and Sawyer, D.A., 1985, Mesozoic ash-flow caldera fragments in southeastern Arizona and their relation to porphyry copper deposits: *Geology*, v. 13, p. 652–656, [https://doi.org/10.1130/0091-7613\(1985\)13<652:MACFIS>2.0.CO;2](https://doi.org/10.1130/0091-7613(1985)13<652:MACFIS>2.0.CO;2).
- Liu, L., Spasojević, S., and Gurnis, M., 2008, Reconstructing Farallon plate subduction beneath North America back to the Late Cretaceous: *Science*, v. 322, no. 5903, p. 934–938.
- Liu, L., Gurnis, M., Seton, M., Saleeby, J., Müller, R.D., and Jackson, J.M., 2010, The role of oceanic plateau subduction in the Laramide orogeny: *Nature Geoscience*, v. 3, p. 353–357, <https://doi.org/10.1038/ngeo829>.
- Livaccari, R.F., Burke, K., and Şengör, A.M.C., 1981, Was the Laramide orogeny related to subduction of an oceanic plateau? *Nature*, v. 289, p. 276–278.
- Lucas, S.G., and Heckert, A.B., 2005, Distribution, age and correlation of Cretaceous fossil vertebrates from Arizona: *New Mexico Museum of Natural History and Science Bulletin*, p. 105–110.
- Ludwig, K.R., 2003, *Isoplot 3.00*: Berkeley Geochronology Center Special Publication No. 4, 70 p.
- Lunt, I.A., Bridge, J.S., and Tye, R.S., 2004, A quantitative, three-dimensional depositional model of gravely braided rivers: *Sedimentology*, v. 51, p. 377–414, <https://doi.org/10.1111/j.1365-3091.2004.00627.x>.
- Mack, G.H., and Rasmussen, K.A., 1984, Alluvial-fan sedimentation of the Cutler Formation (Permo-Pennsylvanian) near Gateway, Colorado: *Geological Society of America Bulletin*, v. 95, p. 109–116, [https://doi.org/10.1130/0016-7606\(1984\)95%3C109:ASOTCF%3E2.0.CO;2](https://doi.org/10.1130/0016-7606(1984)95%3C109:ASOTCF%3E2.0.CO;2).
- Mack, G.H., James, W.C., and Monger, H.C., 1993, Classification of paleosols: *Geological Society of America Bulletin*, v. 105, p. 129–136, [https://doi.org/10.1130/0016-7606\(1993\)105<0129:COP>2.3.CO;2](https://doi.org/10.1130/0016-7606(1993)105<0129:COP>2.3.CO;2).

- Magnani, M.B., Miller, K.C., Levander, A., and Karlstrom, K.E., 2004, The Yavapai-Mazatzal boundary: A long-lived tectonic element in the lithosphere of southwestern North America: *Geological Society of America Bulletin*, v. 116, p. 1137–1142, <https://doi.org/10.1130/B25414.1>.
- Mako, C.A., Williams, M.L., Karlstrom, K.E., Doe, M.F., Powicki, D., Holland, M.E., Gehrels, G.E., and Pecha, M., 2015, Polyphase Proterozoic deformation in the Four Peaks area, central Arizona, and relevance for the Mazatzal orogeny: *Geosphere*, v. 11, p. 1975–1995, <https://doi.org/10.1130/GES01196.1>.
- Martini, M., Solari, L., and López-Martínez, M., 2014, Correlating the arperos basin from Guanajuato, central Mexico, to Santo Tomás, southern Mexico: Implications for the paleogeography and origin of the Guerrero terrane: *Geosphere*, v. 10, p. 1385–1401, <https://doi.org/10.1130/GES01055.1>.
- Marvin, R., Stern, M., Creasey, S.C., and Mehnert, H., 1973, Radiometric ages of igneous rocks from Pima, Santa Cruz, and Cochise Counties, southeastern Arizona: *U.S. Geological Survey Bulletin*, v. 1379, p. 27, <https://doi.org/10.1017/CBO9781107415324.004>.
- McCord, R.D., 1997, An Arizona Titanosaurid Sauropod and Revision of the Late Cretaceous Adobe Canyon Fauna: *Journal of Vertebrate Paleontology*, v. 17, p. 620–622.
- McMillan, N.J., 2004, Magmatic record of Laramide subduction and the transition to Tertiary extension: Upper Cretaceous through Eocene igneous rocks in New Mexico, in Mack, G.H., and Giles, K.A., eds., *The Geology of New Mexico: A Geologic History*: New Mexico Geological Society Special Publication, v. 11, p. 249–270.
- Merewether, E.A., and McKinney, K.C., 2015, Chronostratigraphic cross section of Cretaceous formations in western Montana, western Wyoming, eastern Utah, northeastern Arizona, and northwestern New Mexico, U.S.A.: *U.S. Geological Survey Open-File Report 2015–1087*, 10 p., 1 sheet, <https://dx.doi.org/10.3133/ofr20151087>.
- Miall, A.D., 1977, A review of the braided-river depositional environment: *Earth-Science Reviews*, v. 13, p. 1–62, [https://doi.org/10.1016/0012-8252\(77\)90055-1](https://doi.org/10.1016/0012-8252(77)90055-1).
- Miall, A.D., 1978, Fluvial sedimentology, in Miall, A.D., ed., *Fluvial Sedimentology: An Historical Review*: Canadian Society of Petroleum Geologists Memoir 5, p. 1–47.
- Miall, A.D., 1985, Architectural-element analysis: A new method of facies analysis applied to fluvial deposits: *Earth-Science Reviews*, v. 22, p. 261–308, [https://doi.org/10.1016/0012-8252\(85\)90001-7](https://doi.org/10.1016/0012-8252(85)90001-7).
- Miall, A.D., 1996, *The Geology of Fluvial Deposits*: Berlin, Heidelberg, Springer, 582 p., <https://doi.org/10.1007/978-3-662-03237-4>.
- Miller, H.W., Jr., 1964, Cretaceous dinosaurian remains from southern Arizona: *Journal of Paleontology*, v. 38, p. 378–384.
- Mizer, J.D., 2018, Early Laramide magmatism in southern Arizona; U-Pb geochronology of key igneous units and implications for the timing of regional porphyry copper mineralization [Ph.D. thesis]: Tucson, University of Arizona.
- Nemec, W., and Steel, R.J., 1984, Alluvial and coastal conglomerates: Their significant features and some comments on gravelly mass-flow deposits: *Canadian Society of Petroleum Geologists Memoir*, v. 10, p. 1–31.
- Paces, J.B., and Miller, J.D., 1993, Precise U-Pb Ages of the Duluth Complex and Related Mafic Intrusions, Northeastern Minnesota: *Geochronological Insights to Physical, Petrogenetic, Paleomagnetic, and Tectonomagmatic Processes Associated With the 1.1 Ga Midcontinent Rift System*: *Journal of Geophysical Research*, v. 98, p. 13,997–14,013.
- Pullen, A., Ibáñez-Mejía, M., Gehrels, G.E., Giesler, D., and Pecha, M., 2018, Optimization of a laser ablation-single collector-inductively coupled plasma-mass spectrometer (Thermo Element 2) for accurate, precise, and efficient zircon U-Th-Pb geochronology: *Geochemistry, Geophysics, Geosystems*, v. 19, p. 3689–3705, <https://doi.org/10.1029/2018GC007889>.
- Rasmussen, H., 2000, Nearshore and alluvial facies in the Sant Llorenç del Munt depositional system: Recognition and development: *Sedimentary Geology*, v. 138, p. 71–98, [https://doi.org/10.1016/S0037-0738\(00\)00144-5](https://doi.org/10.1016/S0037-0738(00)00144-5).
- Reiners, P.W., and Brandon, M.T., 2006, Using thermochronology to understand orogenic erosion: *Annual Review of Earth and Planetary Sciences*, v. 34, p. 419–466, <https://doi.org/10.1146/annurev.earth.34.031405.125202>.
- Reiners, P.W., Spill, T.L., Nicolescu, S., and Zanetti, K.A., 2004, Zircon (U-Th)/He thermochronometry: He diffusion and comparisons with $^{40}\text{Ar}/^{39}\text{Ar}$ dating: *Geochimica et Cosmochimica Acta*, v. 68, p. 1857–1887, <https://doi.org/10.1016/j.gca.2003.10.021>.
- Reynolds, S.J., 1980, *Geologic framework of west-central Arizona*: Jenney, J.P., and Stone, C., eds., *Studies in Western Arizona*: Tucson, Arizona Geological Society Digest, v. 12, p. 1–16.
- Scarborough, R., 1989, Cenozoic erosion and sedimentation in Arizona, in Jenney, J.P., and Reynolds, S.J., eds., *Geologic evolution of Arizona*: Tucson, Arizona Geological Society Digest 17, p. 515–537.
- Ridgway, K.D., and DeCelles, P.G., 1993, Stream-dominated alluvial fan and lacustrine depositional systems in Cenozoic strike-slip basins, Denali fault system, Yukon Territory, Canada: *Sedimentology*, v. 40, p. 645–666, <https://doi.org/10.1111/j.1365-3091.1993.tb01354.x>.
- Riggs, N.R., and Busby-Spera, C.J., 1990, Evolution of a multi-vent volcanic complex within a subsiding arc graben depression: Mount Wrightson Formation, Arizona: *Geological Society of America Bulletin*, v. 102, p. 1114–1135, [https://doi.org/10.1130/0016-7606\(1990\)102<1114:EOAMVV>2.3.CO;2](https://doi.org/10.1130/0016-7606(1990)102<1114:EOAMVV>2.3.CO;2).
- Riggs, N.R., Sanchez, T.B., and Reynolds, S.J., 2020, Evolution of the early Mesozoic Cordilleran arc: The detrital zircon record of back-arc basin deposits, Triassic Buckskin Formation, western Arizona and southeastern California, USA: *Geosphere*, v. 16, p. 1042–1057, <https://doi.org/10.1130/GES02193.1>.
- Riley, B.C.D., 2004, Laramide exhumation and heating in southeastern Arizona: Low-temperature thermal history and implications for zircon fission-track systematics [Ph.D. thesis]: Austin, Texas, University of Texas at Austin, 242 p.
- Saleeby, J., 2003, Segmentation of the Laramide slab—Evidence from the southern Sierra Nevada region: *Geological Society of America Bulletin*, v. 115, p. 655–668, [https://doi.org/10.1130/0016-7606\(2003\)115<0655:SOTLSF>2.0.CO;2](https://doi.org/10.1130/0016-7606(2003)115<0655:SOTLSF>2.0.CO;2).
- Saylor, J.E., and Sundell, K.E., 2016, Quantifying comparison of large detrital geochronology data sets: *Geosphere*, v. 12, p. 203–220, <https://doi.org/10.1130/GES01237.1>.
- Saylor, J.E., Jordan, J.C., Sundell, K.E., Wang, X., Wang, S., and Deng, T., 2018, Topographic growth of the Jishi Shan and its impact on basin and hydrology evolution, NE Tibetan Plateau: *Basin Research*, v. 30, p. 544–563, <https://doi.org/10.1111/bre.12264>.
- Seymour, N.M., Strickland, E.D., Singleton, J.S., Stockli, D.F., and Wong, M.S., 2018, Laramide subduction and metamorphism of the Orocochia Schist, northern Plooma Mountains, west-central Arizona: Insights from zircon U-Pb geochronology: *Geology*, v. 46, p. 847–850, <https://doi.org/10.1130/G45059.1>.
- Shaw, C.A., Heizler, M.T., and Karlstrom, K.E., 2005, $^{40}\text{Ar}/^{39}\text{Ar}$ thermochronologic record of 1.45–1.35 Ga intracontinental tectonism in the southern Rocky mountains: Interplay of conductive and advective heating with intracontinental deformation, in Kalstrom, K.E., and Keller, G.R., eds., *The Rocky Mountain Region: An Evolving Lithosphere*: Tectonics, Geochemistry, and Geophysics: Washington, D.C., American Geophysical Union Geophysical Monograph Series, v. 154, p. 163–184, <https://doi.org/10.1029/154GM12>.
- Shaw, C.A., and Karlstrom, K.E., 1999, The Yavapai-Mazatzal crustal boundary in the Southern Rocky Mountains: *Rocky Mountain Geology*, v. 34, p. 37–52, <https://doi.org/10.2113/34.1.37>.
- Snyder, W.S., Dickinson, W.R., and Silberman, M.L., 1976, Tectonic implications of space-time patterns of Cenozoic magmatism in the western United States: *Earth and Planetary Science Letters*, v. 32, p. 91–106, [https://doi.org/10.1016/0012-821X\(76\)90189-8](https://doi.org/10.1016/0012-821X(76)90189-8).
- Spencer, J.E., Richard, S.M., Gehrels, G.E., Gleason, J.D., and Dickinson, W.R., 2011, Age and tectonic setting of the Mesozoic McCoy Mountains Formation in western Arizona, USA: *Geological Society of America Bulletin*, v. 123, p. 1258–1274, <https://doi.org/10.1130/B30206.1>.
- Stewart, J.H., Gehrels, G.E., Barth, A.P., Link, P.K., Christie-Blick, N., and Wrucke, C.T., 2001, Detrital zircon provenance of Mesoproterozoic to Cambrian arenites in the Western United States and Northwestern Mexico: *Geological Society of America Bulletin*, v. 113, p. 1343–1356, [https://doi.org/10.1130/0016-7606\(2001\)113<1343:DZPOMT>2.0.CO;2](https://doi.org/10.1130/0016-7606(2001)113<1343:DZPOMT>2.0.CO;2).
- Stoyanow, A.A., 1949, Lower Cretaceous Stratigraphy in Southeastern Arizona: *Geological Society of America Memoir* 38, 169 p.
- Strecker, M.R., Hilley, G.E., Bookhagen, B., and Sobel, E.R., 2012, Structural, geomorphic, and depositional characteristics of contiguous and broken foreland basins: Examples from the eastern flanks of the Central Andes in Bolivia and NW Argentina, in Busby, C., and Azor, A., eds., *Tectonics of Sedimentary Basins: Recent Advances*: Oxford, Blackwell Publishing, Ltd., p. 508–521, <https://doi.org/10.1002/9781444347166.ch25>.
- Tabor, N.J., Montanez, I.P., Scotese, C.R., Poulsen, C.J., and Mack, G.H., 2008, Paleosol archives of environmental and climatic history in palaeotropical western Pangea during the latest Pennsylvanian through Early Permian, in Fielding, C.R., Frank, T.D., and Isbell, J.L., eds., *Resolving the Late Paleozoic Ice Age in Time and Space*: *Geological Society of America Special Paper* 441, p. 291–303, [https://doi.org/10.1130/2008.2441\(20\)](https://doi.org/10.1130/2008.2441(20)).
- Tarduno, J.A., McWilliams, M., Debiche, M.G., Sliter, W.V., and Blake, M.C., Jr., 1985, Franciscan Complex Calera limestones: Accreted remnants of Farallon Plate oceanic plateaus: *Nature*, v. 317, p. 345–347, <https://doi.org/10.1038/317345a0>.
- Thomas, S.G., Neil, J.T., Myers, T.S., Yang, Y., Wang, D., 2011, Paleosol stratigraphy across the Permian–Triassic boundary, Bogda Mountains, NW China: Implications for palaeoenvironmental transition through earth's largest mass extinction: *Palaeogeography, Palaeoclimatology, Palaeoecology*, v. 308, p. 31–46.
- Titley, S.R., 1976, Evidence for a Mesozoic linear tectonic pattern in southeastern Arizona, in Wilt, J.C., and Jenney, J.P., eds., *Tectonic Digest*: Tucson, Arizona Geological Society Digest, v. 10, p. 71–101.
- Tosdal, R.M., and Stone, P., 1994, Stratigraphic relations and U-Pb geochronology of the Upper Cretaceous upper McCoy Mountains Formation, southwestern Arizona: *Geological Society of America Bulletin*, v. 106, p. 476–491, [https://doi.org/10.1130/0016-7606\(1994\)106<0476:SRAUPG>2.3.CO;2](https://doi.org/10.1130/0016-7606(1994)106<0476:SRAUPG>2.3.CO;2).
- Vermeesch, P., 2013, Multi-sample comparison of detrital age distributions: *Chemical Geology*, v. 341, p. 140–146, <https://doi.org/10.1016/j.chemgeo.2013.01.010>.
- Vervoort, J.D., and Patchett, P.J., 1996, Behavior of hafnium and neodymium isotopes in the crust: Constraints from Precambrian crustally derived granites: *Geochimica et Cosmochimica Acta*, v. 60, p. 3717–3733, [https://doi.org/10.1016/0016-7037\(96\)00201-3](https://doi.org/10.1016/0016-7037(96)00201-3).
- Walker, J.D., Geissman, J.W., Bowring, S.A., and Babcock, L.E., compilers, 2018, *Geologic Time Scale v. 5.0*: *Geological Society of America*, <https://doi.org/10.1130/2018.CTS005R3C>.
- Weil, A.B., and Yankee, W.A., 2012, Layer-parallel shortening across the Sevier fold-thrust belt and Laramide foreland of Wyoming: Spatial and temporal evolution of a complex geodynamic system: *Earth and Planetary Science Letters*, v. 357–358, p. 405–420, <https://doi.org/10.1016/j.epsl.2012.09.021>.
- Whitmeyer, S.J., and Karlstrom, K.E., 2007, Tectonic model for the Proterozoic growth of North America: *Geosphere*, v. 3, p. 220–259, <https://doi.org/10.1130/GES00055.1>.

SCIENCE EDITOR: ROB STRACHAN
ASSOCIATE EDITOR: ERIC ROBERTS

MANUSCRIPT RECEIVED 29 JUNE 2020
REVISED MANUSCRIPT RECEIVED 11 SEPTEMBER 2020
MANUSCRIPT ACCEPTED 6 NOVEMBER 2020

Printed in the USA